Pyroxenite xenoliths and clinopyroxene megacrysts from the Cenozoic Jbel Saghro Volcanic Field (Anti-Atlas, Morocco): Petrography, mineral chemistry and equilibration conditions

Abdelghani Soukrati, Nasrrddine Youbi, Michel Grégoire, Julien Berger, Moulay Ahmed Boumehdi, Abderrahmane Ibhi, Khalid Rkha Chaham

Journal Pre-proof

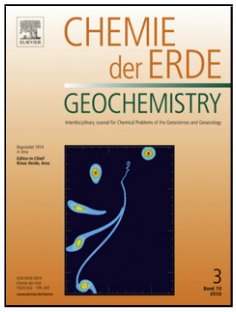

Pyroxenite xenoliths and clinopyroxene megacrysts from the Cenozoic Jbel Saghro Volcanic Field (Anti-Atlas, Morocco): Petrography, mineral chemistry and equilibration conditions

Abdelghani Soukrati (Investigation) (Formal analysis) (Writing - original draft) (Writing - review and editing) (Visualization), Nasrrddine Youbi (Supervision) (Conceptualization), Michel Grégoire (Writing - review and editing) (Validation), Julien Berger (Validation), Moulay Ahmed Boumehdi (Project administration), Abderrahmane Ibhi (Resources), Khalid Rkha Chaham (Writing - original draft)

PII: S0009-2819(20)30105-7

DOI: https://doi.org/10.1016/j.chemer.2020.125694

Reference: CHEMER 125694

To appear in: *Geochemistry*

Received Date: 18 March 2020

Revised Date: 20 September 2020

Accepted Date: 6 October 2020

Please cite this article as: Soukrati A, Youbi N, Grégoire M, Berger J, Boumehdi MA, Ibhi A, Chaham KR, Pyroxenite xenoliths and clinopyroxene megacrysts from the Cenozoic Jbel Saghro Volcanic Field (Anti-Atlas, Morocco): Petrography, mineral chemistry and equilibration conditions, *Geochemistry* (2020), doi: https://doi.org/10.1016/j.chemer.2020.125694

Pyroxenite xenoliths and clinopyroxene megacrysts from the Cenozoic Jbel Saghro Volcanic Field (Anti-Atlas, Morocco): Petrography, mineral chemistry and equilibration conditions

Abdelghani Soukrati[1], Nasrrddine Youbi[1], Michel Grégoire[2], Julien Berger[2], Moulay Ahmed Boumehdi[1], Abderrahmane Ibhi[3], Khalid Rkha Chaham[1]

[1]Department of Geology, Faculty of Sciences-Semlalia, Cadi Ayyad University, Prince Moulay Abdellah Boulevard, P.O. Box 2390, Marrakesh, Morocco, a.soukrati@gmail.com, youbi@uca.ma, boumehdi@uca.ac.ma, rkha@uca.ac.ma

[2]GET, Université de Toulouse, CNRS-CNES-IRD-Université Paul Sabatier, OMP, 14 Av.E. Belin 31400 Toulouse, France, michel.gregoire@get.omp.eu , julien.berger@get.omp.eu,

[3]Department of Geology, Faculty of Sciences, Ibno Zohr University, P.O. Box 28/S, Agadir, Morocco a.ibhi@uiz.ac.ma

*Corresponding author: Abdelghani Soukrati, a.soukrati@gmail.com

Running title: "Pyroxenite xenoliths and megacrysts of Jbel Saghro"

Highlights

- Compositional diversity of pyroxenite xenoliths and clinopyroxene megacrysts in Saghro nephelinites is shown
- Mg-number and Cr_2O_3 contents of clinopyroxene increase from kaersutite-bearing clinopyroxenites to olivine clinopyroxenites
- Chemical compositions of clinopyroxene are used to identify the parental melt of pyroxenite xenoliths and clinopyroxene megacrysts.
- Crystallization of pyroxenite xenoliths and clinopyroxene megacrysts at a wide range of pressure (0.3-0.8 GPa).

Abstract

A suite of mafic pyroxenite xenoliths and clinopyroxene megacrysts was brought to the surface by Cenozoic nephelinites of the Jbel Saghro Volcanic Field (Anti-Atlas, Morocco). The large

population of samples was subdivided into five groups: (i) clinopyroxenites sensu stricto; (ii) olivine clinopyroxenites; (iii) mica-bearing clinopyroxenites; (iv) kaersutite-bearing clinopyroxenites; (v) clinopyroxene megacrysts. These xenoliths display a cumulate texture (adcumulate, heteradcumulate with poikilitic clinopyroxene including olivine). The clinopyroxenes have the composition of augite and show an appreciable variation of MgO (7.02-14.80 wt.%), TiO_2 (0.58-5.76 wt.%) and Al_2O_3 (2.81-12.38 wt.%) contents in grains. The clinopyroxenes are characterized by convex upward chondrite-normalized REE patterns, they display very similar trace element compositions with low contents of incompatible elements such as Rb (0-0.9 ppm), Ba (0.1-8.3 ppm), Th (0.1-0.3 ppm), U (0.01-0.04 ppm) and Nb (1.3-3.2 ppm). REE contents of the calculated melts in equilibrium with the clinopyroxene megacrysts and clinopyroxene from pyroxenite xenoliths are similar to those of the nephelinites exposed in Jbel Saghro. Crystallization temperatures of pyroxenite xenoliths and clinopyroxene megacrysts range from 950 °C to 1150 °C. Clinopyroxene barometry yielded pressure of crystallization ranging from 0.4 to 0.8 GPa for pyroxenite xenoliths and 0.3 to 0.7 GPa for clinopyroxene megacrysts. This pressure range is in agreement with pyroxenite xenoliths and clinopyroxene megacrysts being crystallized from their parental melts at the lower and upper crust.

Keywords

Xenoliths, Pyroxenites, Megacrysts, Trace elements, Nephelinite, Morocco

1. Introduction

Megacrysts of clinopyroxene, amphibole, and olivine commonly occur with pyroxenite xenoliths in alkali basalt, basanitic and nephelinitic lavas (Irving and Frey, 1984; Akinin et al., 2005; Shaw and Eyzaguirre, 2000). The megacrysts are considered to be either high-pressure phenocrysts crystallized from the host basalts (e.g. Binns et al., 1970; Irving and Frey, 1984; Schulze, 1987) or as disrupted fragments of pegmatitic veins and cumulates crystallised from mafic magmas (e.g. Schulze, 1987; Righter and Carmichael, 1993; Shaw and Eyzaguirre, 2000; Ashchepkov et al., 2011). Clinopyroxene megacrysts in alkaline volcanic rocks are an important source of information about the geochemistry of melts and the evolution of magmatic systems (e.g. Dobosi and Jenner, 1999).

Pyroxenites are a volumetrically small, but petrologically significant, mantle/crust rock type. The pyroxenite xenoliths are interpreted as : (i) upper mantle or lower crustal cumulates (crystal segregation from melts) (e.g. Wilkinson, 1975; Wilshire and Shervais, 1975; Choi and Kim, 2012) or (ii) crystallised in magma chambers (e.g. Wilkinson and Stolz, 1997; Villaseca et al., 2019). The

nature and origin of crustal pyroxenites is still largely debated (e.g. Downes, 1993), they constitute a valuable source of information about the nature and evolution of the upper mantle and lower crust (e.g. Downes, 1993; Orejana et al., 2006). Previous studies have reported pyroxenite xenoliths transported by alkaline melts in different regions from Morocco (Sirwa; Bondi et al., 2002, Middle-Atlas; Raffone et al., 2009). The only recent descriptions in the literature of pyroxenite xenoliths and clinopyroxene megacrysts exhumed by the volcanism in the Jbel Saghro are those of Ibhi. (2000).

The Saghro nephelinites host a large diversity of clinopyroxenite xenoliths and clinopyroxene megacrysts that could shed some light on melt transfer and crystallization process below the Saghro hyperalkaline volcanic system belonging to the so called CiMACI (Circum-Mediterranean Anorogenic Cenozoic Igneous province; Lustrino and Wilson, 2007). In this paper, we present the petrography, the mineral major and trace-element compositions for pyroxenite xenoliths and clinopyroxene megacrysts, as well as major elements for olivine megacrysts from Cenozoic Jbel Saghro Volcanic field. The main goals of this work are: (1) to establish equilibration conditions of the pyroxenite xenoliths and clinopyroxene megacrysts, (2) to estimate the parental melt of pyroxenite xenoliths and clinopyroxene megacrysts, and (3) to propose the origin and sequence of crystallization of the investigated samples at various depths.

2. Geological background

The Jbel Saghro Volcanic field (JSVF) is located in eastern part of Moroccan Anti-Atlas representing the northern boundary of the West African Craton (Fig. 1). The Anti-Atlas contains two volcanic edifices: the Sirwa stratovolcano in central Anti-Atlas mainly composed by alkaline to hyperalkaline rocks (basalts, phonolites, and trachytes) and the Jbel Saghro volcanic Field (JSVF) with alkaline nephelinitic, tephritic and phonolitic lavas and domes in the eastern part of Anti-Atlas (Berrahma and Delaloye, 1989; Berrahma et al., 1993). Cenozoic volcanic rocks from the Jbel Saghro (lava flows, necks, minor pyroclastic deposits and domes) are scattered on area of about 50x50 km. These rocks consist of silica-undersaturated nephelinites (olivine nephelinite and pyroxene nephelinite), and phonolites (Berger et al., 2009; Berger et al., 2014). Only one phonotephrite flow is reported in the studied area (Ibhi, 2000; Berger et al., 2014). Tertiary to recent volcanism occurred in two periods (Berrahma et al., 1993): 1) Miocene between 9.6 and 7.6 Ma in the southern part of JSVF; 2) Pliocene-Pleistocene between 5.5 and 2.8 Ma in the northern part of JSVF (Fig.1). The geodynamic setting responsible for the onset of this alkaline magmatism remains a topic of discussion. Considering that the Jbel Saghro volcanic field, the Sirwa stratovolcano and the Canary Islands are aligned and constituted by rocks of similar chemical characteristics, some

authors (e.g. Hoernle and Schmincke, 1993; Ibhi, 2000) have related this volcanism to a mantle plume located at the base of the upper mantle, beneath the Canary Islands. Duggen et al. (2009) proposed that this volcanism was derived from the melting of Canary mantle plume material and its propagation under the Atlasic corridor. In contrast, Liégeois et al. (2005) proposed that the Cenozoic alkaline magmatism of Morocco, occurred along Pan-African or Variscan structures reactivated during the Alpine orogeny, related to the Africa-Europe convergence event. Recently, edge-driven convection process has been proposed as a possible cause of Cenozoic alkaline magmatism located at the northern border of the West African Craton (Missenard and Cadoux, 2011).

3. Sample Descriptions

The samples studied in this work were collected from pyroclastic deposits and lava flows from four areas: Foum el kouss (clinopyroxenites ss, mica-bearing clinopyroxenites, olivine clinopyroxenites, clinopyroxene and olivine megacrysts), Assaka (kaersutite-bearing clinopyroxenites), Tlassem (clinopyroxenites ss and clinopyroxene megacrysts), and Tazlaft Tamzant (clinopyroxene megacrysts). Fifteen pyroxenite xenoliths and five megacrysts were selected from a collection of 40 xenoliths and 20 megacrysts on the basis of optical microscopic examination. The investigated xenoliths are black in color, sub-rounded to elongated in shape and range from 2 to 10 cm in length (Fig. 2). The megacrysts are black or dark green in color, sub-rounded in shape, commonly fractured, and range in length from 1.5 cm to 4 cm. (Fig. 2d, Fig. 3b, and Fig. 3d).

4. Analytical Methods

Major element compositions of mineral were determined with a CAMECA SX Five FE electron microprobe at the Castaing centre (Université Paul Sabatier, Toulouse, France). Analyses have been performed using 15 kV accelerating voltage, 10 to 20 nA beam current, and 10 s/background and peak counting times. The concentrations trace-elements in clinopyroxenes were analysed in situ on 120 µm thick polished sections by LA-ICP-MS at the laboratoire Géosciences environnement Toulouse (GET), Observatoire Midi Pyrénées (Université Paul Sabatier, Toulouse, France). The Thermo Finnigan HR Element XR HR-ICP-MS instrument coupled to a CETAC laser ablation module that uses a 266 nm frequency Nd-YAG laser. The NIST 610 and 612 glass standards were used as external standarts. Each analysis was normalized using CaO values determined by electron microprobe. The analyses were performed on inter-cleavage area from the cores of the fresh clinopyroxene grains in order to get homogeneous results unaffected by alteration

or exsolution processes. A beam diameter of 50 or 100 μm was used for laser ablation spots. The typical relative precision and accuracy for a laser analysis range from 1 to 10%. Each trace element analysis given in the present study corresponds to the average of 2 to 4 analyses of clinopyroxene cores from the same sample.

5. Petrography of host volcanic rocks, xenoliths and megacrysts

5.1. Host rocks

Pyroxenite xenoliths and megacrysts are found in the nephelinite and phonotephrite lava flows from the JSVF. Microscopic observations reveal that the nephelinites (olivine nephelinites and pyroxene nephelinites) have microlitic textures with olivine and clinopyroxene phenocrysts (from 200 to 700 μm in size) within a microcrystalline matrix composed of clinopyroxene, nepheline, Ti-magnetite with minor amounts of apatite, biotite, perovskite, and melilite. The phonotephrite has more or less a dark appearance depending on the proportion of mafic minerals. The phonotephrite consists of resorbed phenocrysts of olivine, clinopyroxene, nosean, nepheline, brown amphibole, and micas. The fine-grained groundmass of this rock consists mainly of sanidine, green pyroxene, nepheline, Ti-magnetite with minor apatite. These host volcanic rocks are described in detail by Ibhi (2000), Berger et al. (2008) and Berger et al. (2009)

5.2. Pyroxenite xenoliths and megacrysts

Mineral composition of the investigated xenoliths is dominated by: clinopyroxene + olivine ± mica ± kaersutite ± nepheline ± spinel. Based on modal compositions, the xenoliths can be classified as clinopyroxenites sensu stricto (ss), olivine clinopyroxenites, mica-bearing clinopyroxenites, and kaersutite-bearing clinopyroxenites (Table 1 and Fig. 4). They prevalently belong to the Group II of xenoliths defined by Frey and Prinz (1978). These xenoliths display cumulate textures (Fig. 3a, Fig. 3c, Fig. 3e, and Fig. 3f) (adcumulate, orthocumulate and heteradcumulate with poikilitic clinopyroxene including olivine grains; e.g. FK28V) except for one sample (AS29) which displays a doleritic texture sensu lato. Coarse clinopyroxene ranges in size from 5 to 15 mm. Spongy texture of the clinopyroxene is more intense close to the contact with the host nephelinite than in the centre of the xenolith. Olivine grain size ranges from 1 to 2 mm, except for one clinopyoxenite (FK28V) which contains olivine up to 14 mm long comprising carbonate inclusions. Mica occurs as subhedral to anhedral cumulus from 1 to 14 mm; mica is surrounded by clinopyroxene crystals and glass (Fig. 3c and Fig. 3f). Kaersutite grains are euhedral to subhedral in shape, with maximum grain size of 6 mm, they are always surrounded by oxide grains in the kaersutite-bearing clinopyroxenites. Brown or opaque spinel forms small interstitial grains (0.5

mm) between large olivine crystals in olivine clinopyroxenites (FK28V). Fine-grained intergranular patches are formed of nepheline, fedspar, secondary clinopyroxene, and carbonate (sample FK28V, F312 and AS29); they are interpreted as an effect of host magma infiltration shortly before eruption or infiltration/percolation of the silica-undersaturated alkali silicate melts (e.g. Matusiak-Malek et al. 2013). Megacrysts of clinopyroxene and olivine are common in the lavas of Jbel Saghro. They belong to the group A, according to the classification of Irving (1984). The megacrysts of clinopyroxene are texturally similar to the clinopyroxene in some of the clinopyroxenites; they display spongy texture in some parts especially near the rim (Fig. 3d). These megacrysts contain some aggregates consisting of euhedral accessory minerals (nepheline, carbonate, zeolite; (TLS1 and F310)) and amphibole (52TT). The presence of these aggregates may be related to direct infiltration of host magma during ascend (e.g. Bonadiman et al. 2011; Puziewicz et al. 2011). The megacrysts of olivine are unzoned and show partial iddingsitization (F1I). In some parts of these megacrysts (F423) a volcanic groundmass with small clinopyroxene and nepheline microlites occurs.

6. Major element mineral chemistry

6.1. Clinopyroxene

Major element composition data for the clinopyroxenes in the nephelinites, pyroxenite xenoliths, and megacrysts are presented in Table 2. For samples F310, TLS1, and F423, the clinopyroxenes from the host volcanic rocks were analyzed.

6.1.1. Host rocks

In the nephelinites, the clinopyroxenes are augites and have a Mg-number [100*Mg/(Mg+Fe_{tot})] ranging from 63 to 83. Cr_2O_3 and TiO_2 contents range respectively from 0.00 to 0.38 wt.% and from 1.01 to 6.06 wt.%. The clinopyroxenes of olivine nephelinites show a wide range of Al_2O_3 and TiO_2 contents than those of clinopyroxenes of pyroxene nephelinites (Fig. 5).

6.1.2. Pyroxenite xenoliths and megacrysts

Clinopyroxenes of the pyroxenite xenoliths are augites with Mg-number ranging from 86 in clinopyroxenes of olivine clinopyroxenite to 44 in clinopyroxenes of kaersutite-bearing clinopyroxenite. They display similar compositions to those of the Al-augite xenoliths reported by Wilshire and Shervais (1975) and the group II xenoliths of Frey and Prinz (1978); which have low MgO (<16 wt.%) and Cr_2O_3 contents (<0.7 wt.%). Al_2O_3 and TiO_2 contents of clinopyroxenes from most samples are relatively heterogeneous, varying respectively from 2.90 to 12.38 wt.% and from 0.58 to 5.76 wt.%. The Cr_2O_3 content of clinopyroxenes in the olivine clinopyroxenites tends to

increase with increasing Mg-number (Fig. 5a), while the Al_2O_3 content of clinopyroxenes in the mica and olivine clinopyroxenites decrease with increasing Mg-number (Fig. 5c). Na_2O content is relatively high for clinopyroxenes in kaersutite-bearing clinopyroxenites (1.47-2.89 wt.%) but low for clinopyroxenes in olivine clinopyroxenites (0.46-1.47 wt.%).

The Mg-number and Cr_2O_3 contents of megacrysts are heterogeneous ranging respectively from 66 to 85 and from 0.00 to 0.58 wt.% (Fig. 5a). They decrease from clinopyroxene megacrysts of Tazlaft Tamzant (84<Mg#<85; Cr_2O_3: 0.46-0.58 wt.%) to clinopyroxene megacrysts of Tlassem area (66<Mg#<74; Cr_2O_3: 0.00-0.01 wt.%). The TiO_2 (1.08-2.29 wt.%) and NaO (0.49-1.75 wt.%) contents of clinopyroxene megacrysts are negatively correlated with Mg-number (Fig.5b and Fig.5d). It should be noticed that the clinopyroxene megacrysts of Tazlaft Tamzant are commonly homogeneous showing no major element variation between core and rim while those from other localities display slight variation of Ti and Al contents between core and rim (Table supplementary data set S1).

6.2. Olivine

6.2.1. Host rocks

In the present study, olivine of olivine nephelinites displays heterogeneous composition (Fo=79 to 90). These values orverlap with the Mg-number field (Fo range from 81 to 88) of olivine from olivine nephelinites evidenced by Berger et al (2008). The NiO and MnO contents are relatively homogeneous, varying respectively from 0.06 to 0.45 wt.% and from 0.12 to 0.92 wt.% (Table 3).

6.2.2. Pyroxenite xenoliths and megacrysts

The olivine phase for the olivine clinopyroxenites (samples FS22, FK29, FK28V, and F312) and olivine megacrysts (samples F423 and F1I) displays homogeneous composition with Mg-number varying respectively from 85 to 87 and from 86 to 88 (Table 3). The NiO content of olivine is lower than 0.29 wt.% in all cases. The CaO content of olivine of olivine clinopyroxenites and megacrysts ranges respectively from 0.20 to 0.45 wt.% and from 0.14 to 0.27 wt.%. In the Fo vs NiO diagram the olivine of olivine clinopyroxenites fall in the fractional accumulation field (Fig. 6). Some olivine megacrysts (sample F423) fall in the fractional accumulation field (Fig. 6) but sample F1I plot within the field of mantle olivines from Takahashi (1987; Fig. 6). Additionally, the high CaO (0.20-0.45 wt.%) of olivine of olivine clinopyroxenites consistent with a cumulate origin and not with an origin from upper mantle (0.05<CaO<0.10; Lee et al., 1996).

Considering the typical composition of the mantle olivine (Fo>89, Ni =0.30 wt.% e.g., Woodland et al., 2006; Lee et al., 1996), the olivine megacryst (F1I) could be derived from a

disaggregation of peridotite xenoliths in magma chamber whereas other olivine megacrysts (sample F423) could be derived from a cumulative rocks.

6.3. Micas

The chemical compositions of the micas are given in the Table 4 and table supplementary data set S3. The structural formulae of micas were calculated on the basis of 22 oxygen.

6.3.1. Host rocks

Micas are found in one sample of olivine nephelinites (Fig. 7a) with Mg-number ranging from 77 to 78. The Al_2O_3 and TiO_2 contents range respectively from 15.43 to 16.06 wt.% and from 6.14 to 6.53 wt.%.

6.3.2. Pyroxenite xenoliths and megacrysts

According to the Speer (1984) diagram (Fig. 7a), micas are phlogopites in olivine clinopyroxenites and kaersutite-bearing clinopyroxenites with Mg-number (74-78). In the mica-bearing clinopyroxenites, these phases are phlogopites in sample F36 (Mg-number = 73-77) but biotites in sample F34 (Mg-number = 65-74). In pyroxenite xenoliths, micas have a narrow range of TiO_2 contents (3.51 to 6.82 wt.%) but a wider range of Al_2O_3 contents (13.30-18.93 wt.%). In addition, the Al_2O_3 contents decrease with increasing MgO (from 14.07 wt.% to 18.62.wt.%) and SiO_2 (from 34.42 to 38.37 wt.%) contents.

6.4. Amphibole

According to the classification of Leake et al. (1997), amphiboles from the studied pyroxenite xenoliths are Ca-amphiboles (kaersutites, Fig. 7b) with Mg-number ranging from 63 to 82 (Table 4). The mica-bearing pyroxenites contain amphiboles with low Mg-number (from 63 to 65), TiO_2 (4.16-5.26 wt.%), and high Al_2O_3 (14.69-15.06 wt.%) contents. The amphiboles of kaersutite-bearing pyroxenites have higher Mg-number (71-74), TiO_2 contents from 4.47 to 5.83 wt.%, and relatively low Al_2O_3 contents (close to 13.11 wt.%). The amphiboles of olivine pyroxenites display highest Mg-number (82), TiO_2 (5.93 wt.%), and low Al_2O_3 (12.25 wt.%) contents. The K_2O contents (1.75-2.67 wt.%) of amphiboles from all pyroxenites are negatively correlated with Mg-number (from 63 to 82) and positively correlated with Al_2O_3 (from 12.25 to 15.06 wt.%).

In the Si versus K+Na+Ca diagram proposed by Sial et al. (1998) and Khezerlou et al. (2017), all the analysed amphiboles fall within the field of magmatic amphiboles. In the Al^{IV}vs Al^{VI}

diagram, the amphiboles from Saghro cumulates fall within the low pressure calcic amphibole field in the sense of Fleet and Barnett, (1978).

6.5. Accessory Phases

Titanite ($CaTiSiO_5$) has been found only in clinopyroxenite ss of the Tlassem area (Sample TLS8; Table 5). It shows homogeneous composition with TiO_2 (37.17-37.87 wt.%), CaO (27.43-27.90 wt.%) and SiO_2 (29.77-29.94 wt.%). Ti-magnetite occurs in the Cpx megacrysts (F310) of Foum el kouss and clinopyroxenite xenoliths of Foum el kouss, Tlassem and Assaka (samples: FS22, TLS8, and AS29; Table 5). The analyses yield 16.00 wt.% of TiO_2, 72.05 wt.% of FeO, 4.94 wt.% of MgO for Ti-magnetite of the Cpx megacrysts, while that of pyroxenites has an average chemical composition of TiO_2=12.50 wt.%, FeO= 73.04 wt.%, MgO= 3.85 wt.%, Al_2O_3 (2.03 wt.%), MnO (1.08 wt.%). Dark spinel only occurs in sample FK28V (olivine clinopyroxenites of Foum el kouss; Table 5). It is a Cr-spinel with Cr# [(100*Cr/Cr+Al)] and Mg-number ranging from 25 to 36 and from 71 to77, respectively. This phase displays low TiO_2 content ranging from 1.36 to 1.86 wt.%, Al_2O_3 (32.14-39.49 wt.%), FeO (21.03-23.88 wt.%), MnO (0.12-0.27 wt.%), and NiO (0.08-0.16 wt.%). In the Cr-number of spinel vs Fo in olivine diagram, cr-spinel plots in crystallization and accumulation processes field. Two rhönite crystals were detected by electron probe in sample F312 (olivine clinopyroxenite). The average chemical composition is: SiO_2 = 25.93 wt.%, FeO = 16.48 wt.%, MgO =16.77 wt.%, CaO = 11.64 wt.%, Al_2O_3 = 15.95 wt.% and TiO_2 = 8.09 wt.%. In this case, the rhönite results from a reaction between kaersutite and host lava, also it could result from decomposition of amphibole (e.g. Shaw, 2009). Small nepheline appears on olivine megacrysts (sample F1I) showing low content of K_2O (3.47 wt.%) while that of olivine clinopyroxenites (sample F312) displays higher content of K_2O (7.89 wt.%). The nepheline of both samples has homogeneous content of Na_2O (15.26-16.18 wt.%). One feldspar crystal (An=0.69; Ab=44.59; Or=54.72) was detected by electron probe in the olivine megacryst (F1I).

7. Trace elements in clinopyroxene

REE and trace element analyses of clinopyroxenes were performed (listed in Table 6) on one biotite-bearing clinopyroxenite (sample F34), two clinopyroxenites ss (samples F440 and TLS8), and one Cpx megacryst (TLS1).

REE patterns of clinopyroxenes from the studied samples are practically identical (Fig. 8a). They are, characterized by enrichment in MREE and depletion in HREE (with $(La/Yb)_N$ and $Ce/Yb)_N$ ratios varying between 4.36-8.14 and 5.98-10.29), similar to those of clinopyroxenes from

pyroxenites crystallized from alkali basalts (e.g. Wilshire and Shervais, 1975; Frey and Prinz, 1978; Suen and Frey, 1987; Perinelli et al., 2011).

In chondrite-normalized trace multi-element diagram, the investigated clinopyroxenes are characterized by a marked depletion in most incompatible elements and strong negative U anomalies; (0.01 ppm of U in sample TLS8 and TLS1; and from 0.02 to 0.04 ppm of U in samples F34 and F440). The Zr concentrations in pyroxenes increase from primitive clinopyroxenes (samples F440; from 87 to 212 ppm of Zr) to the most evolved clinopyroxenes (sample TLS8; from 316 to 409 ppm of Zr) (Fig. 8b and Table 6). The increase of Zr concentrations is already known from other alkaline complexes (e.g. Batki et al. 2018). Additionally, the Ti concentrations are low in the Cpx of clinopyroxenite (TLS8) and Cpx megacryst (TLS1) from Tlassem (9164 to 11904 ppm) but high in Cpx of clinopyroxenite (F440) and biotite-bearing clinopyroxenite (F34) from Foum el kouss (13680.5 to 22382 ppm).

Clinopyroxenes of sample F440 exhibit the highest Mg# (0.78) and low Hf/Sm ratios whereas those of sample TLS8 display the lowest Mg# (0.65) and high Hf/Sm ratios. Overall, the Hf/Sm ratios of Cpx from pyroxenite xenoliths and megacrysts are negatively correlated with Mg-number (Fig.9) suggesting that the clinopyroxenes crystallized from progressively fractionated melts or a parental magma undergoing progressive differentiation (e.g. Woodland and Jugo., 2007).

8. Discussion

The upper mantle beneath the Jbel Saghro Volcanic Field (JSVF) consists of peridotites (mainly spinel-bearing lherzolites (Ibhi and Nachit., 1999; Ibhi, 2000) while this study shows that pyroxenites occur in the crust. Moreover, the pyroxenites and Cpx-megacrysts in alkaline volcanic rocks provide important information on the evolution of melts and magmatic systems (e.g. Dobosi and Jenner, 1999; Berly et al., 2006; Dantas et al., 2009).

The petrography and mineral chemistry data presented in the previous sections allow us to infer the processes involved in the genesis of pyroxenites and megacryts from the Jbel Saghro Volcanic Field (JSVF).

8.1. Levels of crystallization for pyroxenite xenoliths and clinopyroxene megacrysts

Clinopyroxenes from xenoliths show $^{VI}Al/^{IV}Al$ ratios ranging from 0.04 to 0.77, those of clinopyroxene megacrysts vary from 0.10 to 0.64. These values are similar to those of clinopyroxenes from pyroxenite xenoliths (0.24-0.39) reported by Bondi et al. (2002). Thus, these ranges indicate that the studied samples were formed in the crust depths rather than in the mantle.

On the other hand, the clinopyroxenes of the studied samples plot in the field of granulites and inclusions in basalts in the Al^{IV}vsAl^{VI} diagram (Aoki and Shiba, 1973; Fig. 10a).
The pressure and temperature estimates for the studied samples were obtained using the clinopyroxene only (Nimis and Ulmer, 1998) and clinopyroxene-liquid equilibria (Putirka, 2008).

Nimis and Ulmer (1998) proposed calibrations to estimate the pressure of equilibration of magmatic clinopyroxenes such as those occurring in cumulates or as megacrysts in volcanic rocks. The first calibration (BA ; anhydrous alkaline) is independent of the temperature, so the compositional variability of clinopyroxene observed between the investigated samples is a direct reflect of their pressure of equilibration which is also their pressure of crystallization. This calibration provides consistent results within an error range of about 0.17 GPa. The second calibration (BH ; hydrous alkaline) is the best approximation for some of the studied xenoliths (mica and amphibole-bearing pyroxenites). In practice, the use of this second calibration requires knowing the temperature; the most reliable thermometer is the Putirka (2008).
With this geobarometer of Nimis and Ulmer (1998), the clinopyroxene phenocrysts of host rocks record relatively low pressures ranging from 0.3 to 0.4 GPa. Pyroxenite xenoliths yield higher P-estimates ranging from 0.4 to 0.7 GPa (Fig. 10b) but the olivine pyroxenite containing spinel (sample FK28V) equilibrated at around 0.8 GPa. The pressure estimates for the clinopyroxene megacrysts (samples F310 and TLS1) range from 0.1 to 0.3 GPa (Fig. 10c and Table 7), these values are similar to those estimated for the clinopyroxene megacrysts (type 2 and 3) from the Devès Volcanic Field (DVF; East French Central Massif, France; Woodland and Jugo, 2007). The clinopyroxene megacryst (sample 52TT) records a high pressure close to 0.7 GPa overlapping with the range of estimated pressures for the clinopyroxene of type 1a and 1c from the DVF (Woodland and Jugo, 2007). This range (0.4-0.8 Gpa) is compatible with the lack of garnet in all samples that constrains the equilibrium pressures at values lower than 1.4 GPa (e.g. perinelli et al 2011). On the other hand, these estimates therefore show that the pyroxenite xenoliths and clinopyroxene megacrysts from JSVF were formed within the crust. They are lower than values calculated by Berger et al. (2008) (0.98 Gpa at crust-mantle boundary).
Geothermometer of Putirka (2008), based on clinopyroxene-liquid equilibrium, is applied to calculate the crystallization temperature of clinopyroxene in equilibrium with the host lavas. In our case, the parent liquid compositions were approximated using whole-rock compositions of the host lavas studied by Berger et al (2009). Calculated temperatures based on this thermometer of Putirka (2008) range between 950 and 1150 °C for pyroxenite xenolths and megacrysts. These temperatures are similar to those recorded by Ibhi (2000) for pyroxenites from the Saghro area.

8.2. Estimates of Melt in equilibrium with clinopyroxenes and comparison with Moroccan Cenozoic volcanic rocks

The Mg-number of clinopyroxene megacrysts and clinopyroxene from pyroxenites ranges from 44 to 86, whereas the host rocks have Mg# ranging from 60 to 72 (Berger et al. 2009, 2014). This wide range of values suggests that the clinopyroxene has crystallised from moderately differentiated melts to primary melts. We have calculated the REE compositions of theoretical liquids in equilibrium with the clinopyroxene megacryst and clinopyroxene from the pyroxenite xenoliths, based on partition coefficients between the mineral and melt ($D^{cpx/nephelinite}$), using the values from Hart and Dunn (1993: La, Ce, Nd, Sm, Dy, Er, Yb and Lu). The chondrite-normalized rare earth element patterns of the theoretical liquids in equilibrium with the clinopyroxene of pyroxenites and Cpx megacrysts are more or less sub-parallel to those of host nephelinites from Saghro (Berger et al., 2014); and other areas (Middle-Atlas; El Azzouzi et al., (2000), and Estern Morocco; Wagner et al., (2003)) (Fig. 11). This suggests that the pyroxenites and clinopyroxene megacrysts crystalized from melts similar in composition to the host alkaline rocks. The REE concentration levels are slightly higher for the calculated liquids relative to those of volcanic rocks (Fig. 11) indicating that the former are a little bit more evolved than the latter. The clinopyroxenes of investigated samples have theoretical melt patterns very close in term of shape to those of accumulative pyroxenite (sample IBA18) from Bou Ibalghatene from Middle-Atlas (Raffone et al., 2009) and the pyroxenite xenoliths and clinopyroxene megacrysts from Sirwa (Bondi et al., 2002). In summary, the composition of the parental melts calculated from the JSVF pyroxenite xenoliths and Cpx megacrysts indicates that they have a genetic relationship with the Cenozoic-Plio-Quaternary nephelinitic lavas.

8.3. Origin and sequential crystallization of the pyroxenite xenoliths and clinopyroxene megacrysts

The pyroxenite xenoliths and megacrysts from Saghro do not have characteristics of mantle xenoliths, except of the sample F1I (olivine megacryst) could be derived from a peridotite source (disaggregated mantle peridotites, Fig. 6). The clinopyroxene megacrysts and clinopyroxenes from pyroxenites display a major element chemistry overlapping that of clinopyroxenes from nephelinites, this implies that they all must share a magmatic origin and crystallized from similar cogenetic basic melts (Fig. 5). The convex-upward shape of REE patterns of clinopyroxene of samples from the Foum el kouss and Tlassem localities is in agreement with a fractional crystallization process from parental mafic liquids at variable pressures and temperatures (e.g. Frey and Prinz, 1978; Irving and Frey, 1984; Perinelli et al., 2011) and imply that they represent possibly

comagmatic crystallization sequences. (e.g. Batki et al., 2018). The covariation of high field strength elements and REE with Mg#, as exemplified by Hf/Sm, indicates that different pyroxenites and megacrysts crystallized from genetically related magmas that have undergone progressive degrees of differentiation. Sample F34 is an exception to this figure; its Hf/Sm departs from the general linear trend defined by the remaining samples (Fig. 9). The broad similarity between the calculated melts and the Saghro volcanic rocks (Fig. 11) suggests that pyroxenites and clinopyroxene megacrysts crystallized from melts with a composition similar to that of the host alkaline magmas. The variation of Mg-number in clinopyroxenes as a function of pressure is illustrated in Fig. 12. The Mg-number varies between 85.47 (sample FK28V) and 43.72 (sample AS29) at pressure between 0.8 Gpa and 0.1 Gpa. We can explain this marked variation by fractional crystallization in two crustal magma chambers; the first in the lower crust (step 1) the second in the upper crust (step 2 and step 3). This relatively in agrement with the pressures calculated by Berger et al. (2008). In our case, the crystallization sequence of minerals (Fig. 12) is as follows: 1) the early step characterized by abundance of olivine and clinopyroxene with accessory Al-spinel and Ti-magnetite; 2) decreasing Mg-number favors clinopyroxene and micas over olivine; 3) this step characterized by formation of amphibole and phlogopite of kaersutite-bearing clinopyroxenite (AS29) with accessory titanite (TLS8).

In summary, the major and trace element compositions as well as barometric estimates of the clinopyroxene megacrysts and clinopyroxenes from clinopyroxenite xenoliths are consistent with an origin by fractional crystallization, at crustal depths, from alkali melts. This history is an agreement with the ‘mush column’ model of Marsh (1996) evidenced in other areas as Mont Briancon and Marais de Limagne from French Central Massif (Woodland and Jugo, 2007).

9. Conclusion:

Cenozoic nephelinites and tephrites of the Jbel Saghro volcanic field carry a suite of pyroxenite xenoliths and clinopyroxene megacrysts which can be divided into five groups according to their petrological and mineralogical characteristics: (i) clinopyroxenites ss; (ii) olivine clinopyroxenites; (iii) mica-bearing clinopyroxenites; (iv) kaersutite-bearing clinopyroxenites; and (v) clinopyroxene megacrysts. The estimated pressures, ranging from 0.1 to 0.8 GPa, suggest that the pyroxenite xenoliths and clinopyroxene megacrysts from JSVF were formed within the crust. The convex-upward shape of REE patterns of the studied clinopyroxenes is in agreement with a fractional crystallization process from parental mafic liquids at variable pressures and temperatures. The chondrite-normalized rare earth element patterns of the parental melts are more or less sub-parallel

to those of host nephelinites from Saghro. This indicates that the pyroxenites and clinopyroxene megacrysts were crystalized from melts similar in composition to the host alkaline rocks.

CRediT author statement

Abdelghani Soukrati: Investigation, Formal analysis , Writing - Original Draft, Writing - Review & Editing, Visualization.

Nasrrddine Youbi: Supervision, Conceptualization.

Michel Grégoire: Writing - Review & Editing, Validation.

Julien Berger: Validation.

Moulay Ahmed Boumehdi: Project administration.

Abderrahmane Ibhi: Resources.

Khalid Rkha Chaham: Writing - Original Draft.

Declaration of interests

☒The authors declare that they have no known competing financialinterestsor personal relationships that could have appeared to influence the work reported in this paper.

Acknowledgements

This work was financially supported by the French Centre National of Scientific Research (CNRS) and the Moroccan National Centre of Scientific and Technical Research (CNRST) to MG and NY. IRSES MEDYNA programme is thanked for the two months scholarship awarded to the first author for his scientific stay at the Geosciences Environment Toulouse laboratory. We are particularly indebted to Philippe de Parseval and Sophie Gouy for their help during the electron microprobe analyses. We thank the associate editor and two anonymous reviewers, whose comments significantly improved an earlier version of the paper.

References

Akinin, V.V., Sobolev, A.V., Ntaflos, T., Richter, W., 2005. Clinopyroxene megacrysts from Enmelen melanephelinitic volcanoes (Chukchi Peninsula, Russia): application to composition and evolution of mantle melts. Contrib. Mineral. Petrol. 150, 85–101.

Aoki, K. and Shiba, I., 1973. Pyroxene from lherzolites inclusions of Itinomegata, Japan. Lithos 6, 41–51.

Ashchepkov, I.V., André, L., Downes, H., Belyatsky, B.A., 2011. Pyroxenites and megacrysts from Vitim picrite-basalts (Russia): Polybaric fractionation of rising melts in the mantle?. J. Asian Earth Sci. 42, 14–37.

Batki, A., Pál-Molnár, E., Jankovics, M.E., C. Kerr, A., Kiss, B., Markl, G., Heincz, A., Harangi, S., 2018. Insights into the evolution of an alkaline magmatic system: An in situ trace element study of clinopyroxenes from the Ditrău Alkaline Massif, Romania. Lithos 300–301, 51–71.

Berger, J., Ennih, N., Liégeois, J.P., Nkono, C., Mercier, J.C.C., Demaiffe, D., 2008. A complex multichamber magmatic system beneath a late Cenozoic volcanic field: evidence from CSDs and thermobarometry of clinopyroxene from a single nephelinite flow (Djbel Saghro, Morocco). Geol. Soc. London 297, 509–524.

Berger, J., Ennih, N., Mercier, J.C.C., Liégeois, J.P., Demaiffe, D., 2009. The role of fractional crystallization and the late-stage peralkaline melt segregation in the mineralogical evolution of Cenozoic nephelinites/phonolites from Saghro (SE Morocco). Mineral. Mag. 73, 59–82.

Berger, J., Liégois, J.P., Ennih, N., Bonin, B., 2010. Flow of Canary mantle plume material through a subcontinental lithospheric corridor beneath Africa to the Mediterranean: Comment. Geology, 38, e202.

Berger, J., Ennih, N., Liégeois, J.P., 2014. Extreme trace elements fractionation in Cenozoic nephelinites and phonolites from the Moroccan Anti-Atlas (Eastern Saghro). Lithos 210–211, 69–88.

Berly, T.J., Hermann, J., Arculus, R.J., Lapierre, H., 2006. Supra-subduction zone pyroxenites from San Jorge and Santa Isabel (Solomon Islands). J. Petrol. 74, 1531-1555.

Berrahma, M and Delaloye, M., 1989. Données géochronologiques nouvelles sur le massif volcanique du Siroua (Anti-Atlas, Maroc). J. Afr. Earth Sci. 9, 651–656.

Berrahma, M., Delaloye, M., Faure-Muret, A., Rachdi, H.E.N., 1993. Premières données géochronologiques sur le volcanisme alcalin du Jbel Saghro, Anti-Atlas, Maroc. J. Afr. Earth Sci. 17, 333–341.

Binns, R.A., Duggan, M.B., Wilkinson, J.F.G., Kalocsai, G. I. Z., 1970. High-pressure megacrysts in alkaline lavas from northeastern New South Wales. Amer. J. Sci. 269,132–168.

Bonadiman, C., Coltorti, M., Beccaluva, L., Griffin, W.L., O'Reilly, S.Y., Siena, F., 2011. Metasomatism versus host magma infiltration : A case study of Sal mantle xenoliths, Cape Verde Archipelago . Geol. Soc. Am. Spec. Paper 478, 283–305.

Bondi, M., Morten, L., Nimis, P., Rossi, P.L., Tranne, C.A., 2002. Megacrysts and mafic-ultramafic xenoliths-bearing ignimbrites from Sirwa Volcano, Morocco: phase petrology and thermobarometry. Mineral. Petrol. 75, 203–221.

Chamboredon, R., 2015. Caractérisation et origine des magmas alcalins et des fluides sous le massif volcanique du Jbel Saghro, Anti-Atlas, Maroc. Ph.D. thesis, 149p. Montpellier university.

Choi, S.H., Kim, N.K., 2012. Petrogenesis of anhydrous clinopyroxenite xenoliths and clinopyroxene megacrysts in alkali basalts from the Ganseong area of South Korea. Isl. Arc 21,101–117.

Dantas, C., Grégoire, M., Koester,E., Conceição, R.V., Rieck Jr, N. 2009. The lherzolite–websterite xenolith suite from Northern Patagonia (Argentina): Evidence of mantle–melt reaction processes. Lithos 107, 107–120

Dobosi, G. and Jenner, G.A., 1999. Petrologic implications of trace element variation in clinopyroxene megacrysts from the Nógrád volcanic province, north Hungary: a study by laser ablation microprobe-inductively coupled plasma-mass spectrometry. Lithos 46,731–749.

Downes, H., 1993. The nature of the lower continental crust of Europe; petrological and geochemical evidence from xenoliths. Phys. Earth Planet. Inter. 79,195–218.

Duggen, S., Hoernle, K.A., Hauff, F., Klugel, A., Bouabdellah, M., Thirlwall, M.F., 2009. Flow of Canary mantle plume material through a subcontinental lithospheric corridor beneath Africa to the Mediterranean. Geol. 37, 283–286.

El Azzouzi, M., Maury, R.C., Bellon, H., Youbi, N., Cotten, J., Kharbouch, F., 2010. Petrology and K-Ar chronology of the Neogene-Quaternary Middle Atlas basaltic province, Morocco. Bull. Soc. Geol. Fr. 181 (3), 243-257.

Fleet, M.E and Barnett, R.L., 1978. Al $^{(IV)}$/Al $^{(VI)}$ partitioning in calciferous amphiboles from the mine, Sudbury, Ontario. Can. Mineral. 16, 527–532.

Frey, F.A. and Prinz, M., 1978. Ultramafic inclusions from San Carlos, Arizona: petrological and geochemical data bearing on their petrogenesis. Earth Planet. Sci. Lett. 38, 129–176.

Hart, S.R. and Dunn, T., 1993. Experimental Cpx/melt partitioning of 24 trace elements. Contrib. Mineral. Petrol. 113, 1–8.

Hoernle, K. and Schmincke, H.U., 1993. The role of partial melting in the 15-Ma geochemical evolution of Gran-Canaria - a blob model for the Canary hotspot. J. Petrol. 34, 599–626.

Ibhi, A. and Nachit, H., 1999a. Découverte d'une association d'enclaves carbonatite-lherzolite dans le volcanisme plio-quaternaire de Foum El kouss (Jbel Saghro) : mise en place d'un manteau carbonaté à l'aplombe de L'Anti-Atlas Oriental Marocain. Rev. Géol. Méditerr. Tome 26 N° 1–2, 19–28.

Ibhi, A., 2000. Le volcanisme Plio-Quaternaire de Saghro (Anti-Atlas, Maroc) et les enclaves basiques et ultrabasiques associées. Ph.D. thesis, 354 p., Agadir University, Morocco.

Irving, A.J., 1984. Polybaric mixing and fractionation of alkalic magmas: evidence from megacryst suites. EOS Am. Geophys. Union Trans . 65**,** 1153.

Irving, A.J. and Frey, F.A., 1984. Trace element abundances in megacrysts and their host basalts: constraints on partition coefficients and megacrysts genesis. Geochim. Cosmochim. Acta 48, 1201–1221.

Khezerlou, A.A., Amel, N., Grégoire, M., Moayyed, M., Jahangiri, A., 2017. Geochemistry and Mineral chemistry of pyroxenite xenoliths and host volcanic alkaline rocks from North West of Marand (NW Iran). J. Mineral. Petrol. 111, 865–885.

Leake, B.E., Woolley, A.R., Arps, C.E.S et al., 1997. Nomenclature of amphiboles: Report for the subcommittee on amphiboles of the international mineralogical association, commission on a new minerals and mineral names. Can. Mineral. 35, 219–246.

Lee, D.C., Halliday, A.N., Davies, G.R, Essene, E.J., Fitton, G.J., Temdjim, R., 1996. Melt Enrichment of Shallow Depleted Mantle: a Detailed Petrological, Trace Element and Isotopic Study of Mantel-Derived Xenoliths and Megacrysts from the Cameron Line. J. Petrol. 37, 415-441.

Liégeois, J.P., Benhallou, A., Azzouni-Sekkal, A., Yahiaoui, R., Bonin, B., 2005. The Hoggar swell and volcanism; Reactivation of the Precambrian Tuareg shield during Alpine convergence and West African Cenozoic volcanism. Geol. Soc. Am. Spec. Paper 388, 379–400.

Lustrino, M. and Wilson, M., 2007. The Circum-Mediterranean Anorogenic Cenozoic Igneous Province. Earth Sci. Rev. 81, 1–65.

Matusiak-Malek, M., Puziewicz, J., Ntaflos, T., 2013. Origin of integranular aggregates in mantle xenoliths from Krzeniow basanite. Geosci. Notes 1, 25–49.

Marsh, B.D. 1996. Soldification fronts and magmatic evolution. Mineral. Mag. 60, 5–40.

McDonough, W.F. and Sun, S., 1995. The composition of the Earth. Chem. Geol. 120, 223–253.

Missenard, Y. and Cadoux, A., 2012. Can Moroccan Atlas lithospheric thinning and volcanism be induced by Edge-Driven Convection?.Ter. Nova 24, 27–33.

Nimis, P. and Ulmer, P., 1998. Clinopyroxene geobarometry of magmatic rocks Part 1: an expanded structural geobarometer for anhydrous, basic and ultrabasic systems. Contrib. Mineral. Petrol. 133, 122–135.

Orejana, D., Villaseca, C., Paterson, B.A., 2006. Geochemistry of pyroxenitic and hornblenditic xenoliths in alkaline lamprophyres from the Spanish Central System. Lithos 86, 167–196.

Perinelli, C., Armienti, P., Dallai, L., 2011. Thermal evolution of the Lithosphere in a Rift Environment as Inferred from the Geochemistry of Mantle cumulates, Northern Victoria Land, Antarctica. J. Petrol. 52, 665–690.

Putirka, K.D., 2008. Thermometers and Barometers for Volcanic Systems. Rev. Mineral. Geochem. 69, 61–120.

Puziewicz, J., Koepke, J., Grégoire, M., Ntaflos, T., Matusiak-malek, M., 2011. Lithospheric Mantle Modification during Cenozoic Rifting in Central Europe: Evidence from the Ksieginki Nephelinite (SW Poland) Xenolith Suite. J. Petrol. 52, 2107–2145.

Raffone, N., Chazot, G., Pin, C., Vannucci, R., Zanetti, A., 2009. Metasomatism in the Lithospheric Mantle beneath Middle Atlas (Morocco) and the Origin of Fe- and Mg-rich Wehrlites.

J. Petrol. 50, 197–249.

Righter, K. and Carmichael, I. S. E., 1993. Mega-xenocrysts in alkali olivine basalts: fragments of disrupted mantle assemblages. Am. Mineral. 78, 1230–1245.

Schulze, D.J., 1987. Megacrysts from alkalic volcanic rocks. In: Nixon P (ed) Mantle xenoliths. John. Wiley, N. Y. USA. 433–451.

Shaw, C. S. J. and Eyzaguirre, J., 2000. Origin of megacrysts in the mafic alkaline lavas of the West Eifel volcanic field, Germany. Lithos 50, 75–95.

Shaw, C. S. J., 2009. Textural development of amphibole during breakdown reactions in a synthetic peridotite. Lithos 110, 215–228.

Sial, A.N., Ferreira, V.P., Fallick, A.E., Jeronimo, M., Cruz, M., 1998. Amphibole-rich clots in calcalkalic granitoids in the Borborema province northeastern Brazil. J. S. Am. Earth Sci. 11, 457–471.

Speer, J.A., 1984. Micas in igneous Rocks. In Bailey. S.W (ed) Micas. Rev Mineral. 13, 299–356.

Suen, C.J and Frey, F.A., 1987. Origins of mafic and ultramafic rocks in the Ronda peridotites. Earth Planet. Sci. Lett. 85, 183–202.

Takahashi, E. 1986. Origin of basaltic magmas-implication from peridotite melting experiments and olivine fractionation model. Bull. Volcanol. Soc. Jpn. 30 S17-S40 (In Japanes with English abstract).

Villaseca, C., Dorado, O., Orejana, D., 2019. Mineral chemistry of megacrysts and associated clinopyroxenite enclaves in the Calatrava volcanic field: crystallization processes in mantle magma chambers. J. Iber. Geol. 45, 401–426.

Wagner, C., Deloule, E., Mokhtari, A., 1996. Richterite bearing peridotites and MARID-type inclusions in lavas from North Eastern Morocco: Mineralogy and D/H isotopic studies. Contrib. Mineral. Petrol. 124, 406–421.

Wilkinson, J. F. G., 1975. Ultramafic inclusions an high pressure megacrysts from a nephelinite sill, Nandewar Mountains, north-eastern New South Wales, and their bearing on the origin of certain ultramafic inclusions in alkaline volcanic rocks. Contrib. Mineral. Petrol. 51, 235–262

Wilkinson, J.F.G. and Stolz, A.J., 1997. Subcalcic clinopyroxenites and associated ultramafic xenoliths in alkali basalt near Glen Innes, Northeastern New South Wales, Australia. Contrib. Mineral. Petrol. 127, 272–291.

Wilshire, H. G. and Shervais, J. W., 1975. Al–augite and Cr–diopside ultramafic xenoliths in basaltic rocks from western United States. Phys. Chem. Earth 9, 257–272.

Woodland, A.B., Kornprobst, J., Tabit, A., 2006. Ferric iron in orogenic lherzolite massifs and controls of oxygen fugacity in the upper mantle. Lithos 89, 222–241.

Woodland, A.B. and Jugo, P.J., 2007. A complex magmatic system beneath the Devès volcanic field, Massif Central, France: evidence from clinopyroxene megacrysts. Contrib. Mineral. Petrol. 153, 719–731.

Figure captions

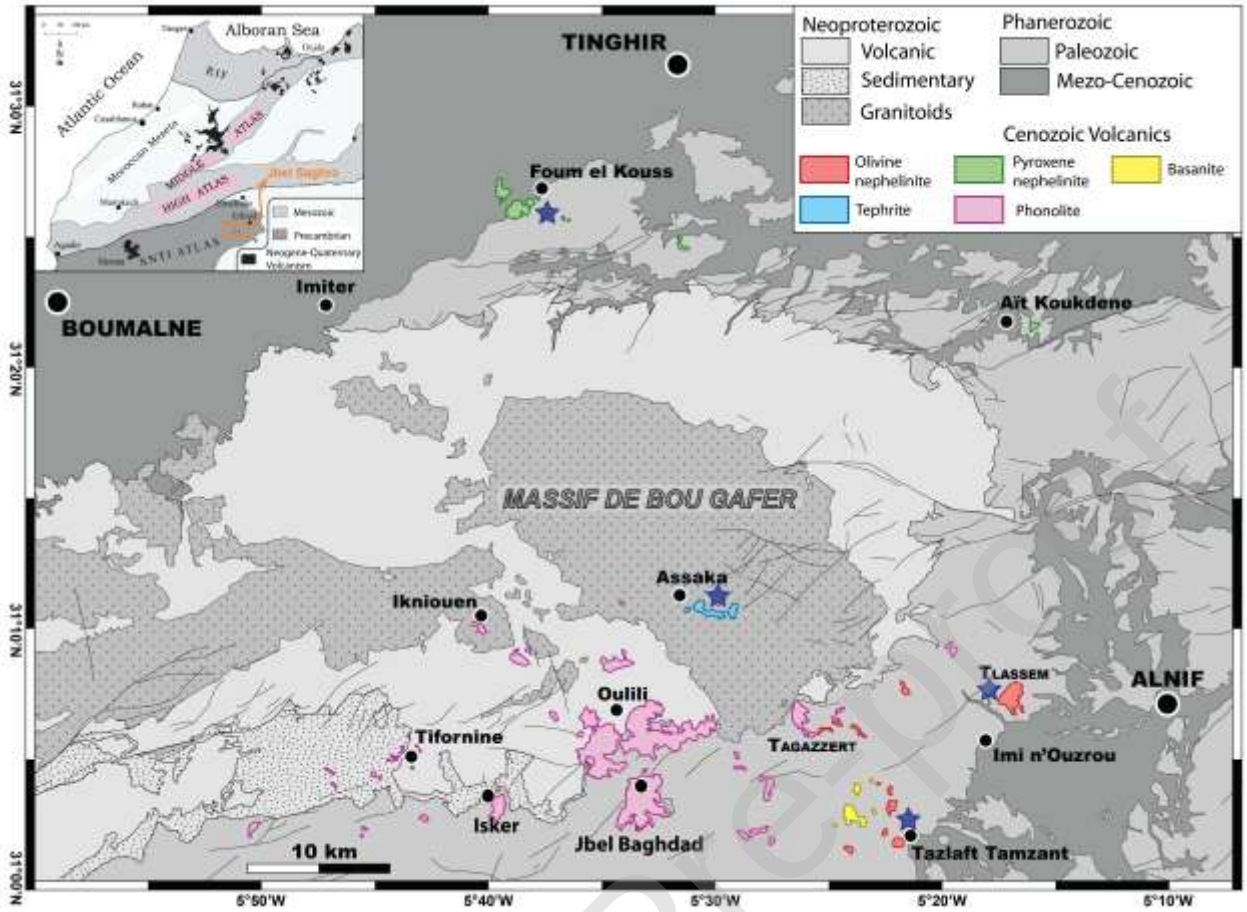

Fig. 1: Geological map of the Jbel Saghro volcanic field (JSVF) showing the location of nephelinites, basanites, tephrites and phonolites (after Chamboredon, 2015). The inset displays the location of the Saghro volcanic field in the Atlas mountain belt, Northwest Africa (modified after El Azzouzi et al., 2010). The stars show the localities where the studied samples in this paper were collected.

Fig. 2: Field photographs of some investigated pyroxenite xenoliths and Cpx megacrysts: a) clinopyroxenite xenoliths (sample F440) in the nephelinite; b) clinopyroxenite xenoliths (sample F444) in the pyroclastic deposits; c) olivine pyroxenite xenoliths (sample FK29) in the nephelinite; d) clinopyroxene megacrysts (sample TLS1) in the nephelinite.

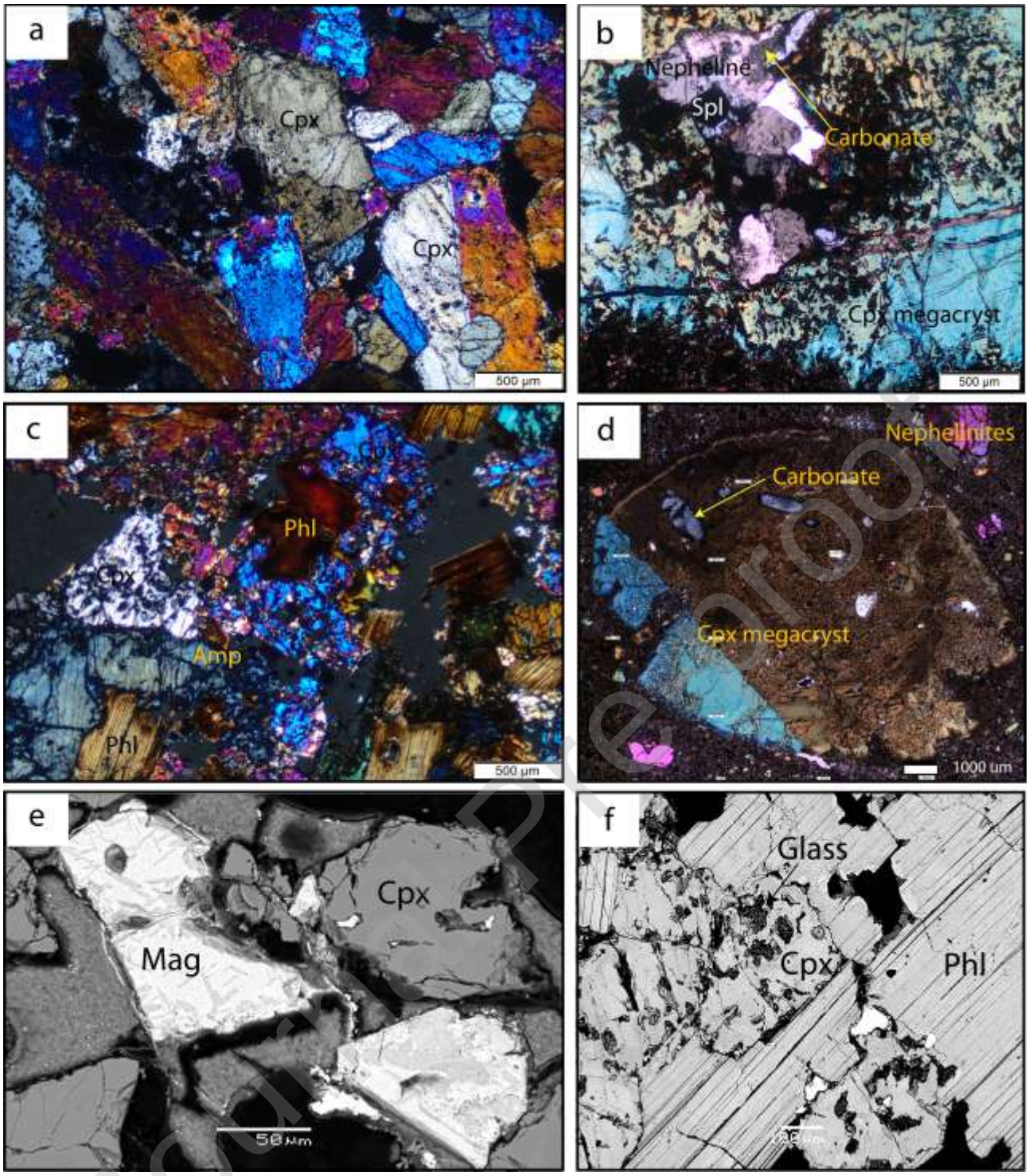

Fig. 3: Photomicrographs of investigated pyroxenite xenoliths and Cpx megacryts: a) and c) cumulative texture in olivine clinopyroxenite (sample FK29) and mica-bearing clinopyroxenite (sample F34); b) Cpx megacrysts (sample F310); d) Cpx megacrysts (sample TLS1) with reaction rim at the contact between the megacrysts and host nephelinite; e and f) back-scattered electron image (BSE) view of texture of cumulate.

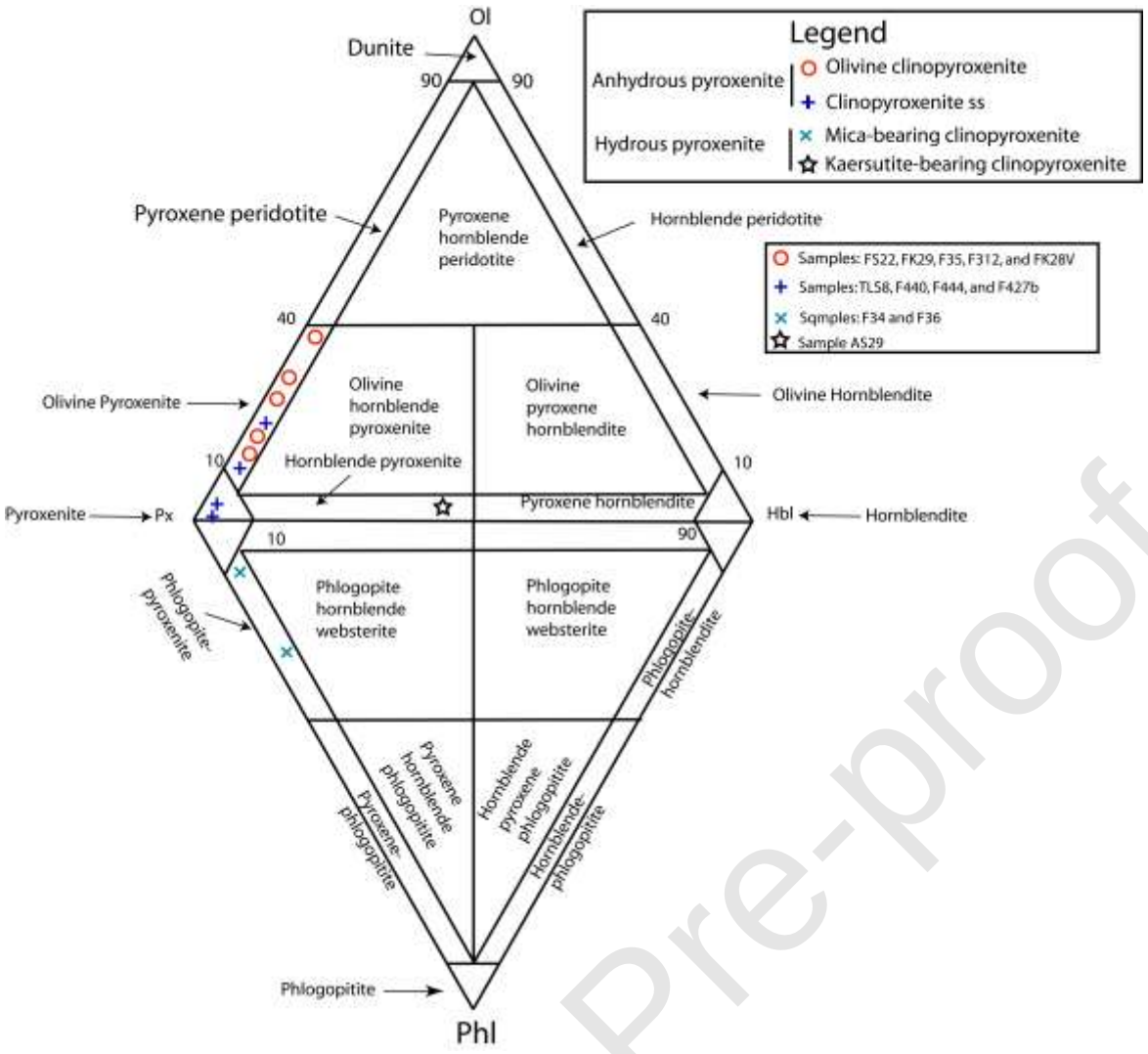

Fig. 4: ”Exploded” faces of the POPH (phlogopite-olivine-pyroxene-hornblende) diagram.

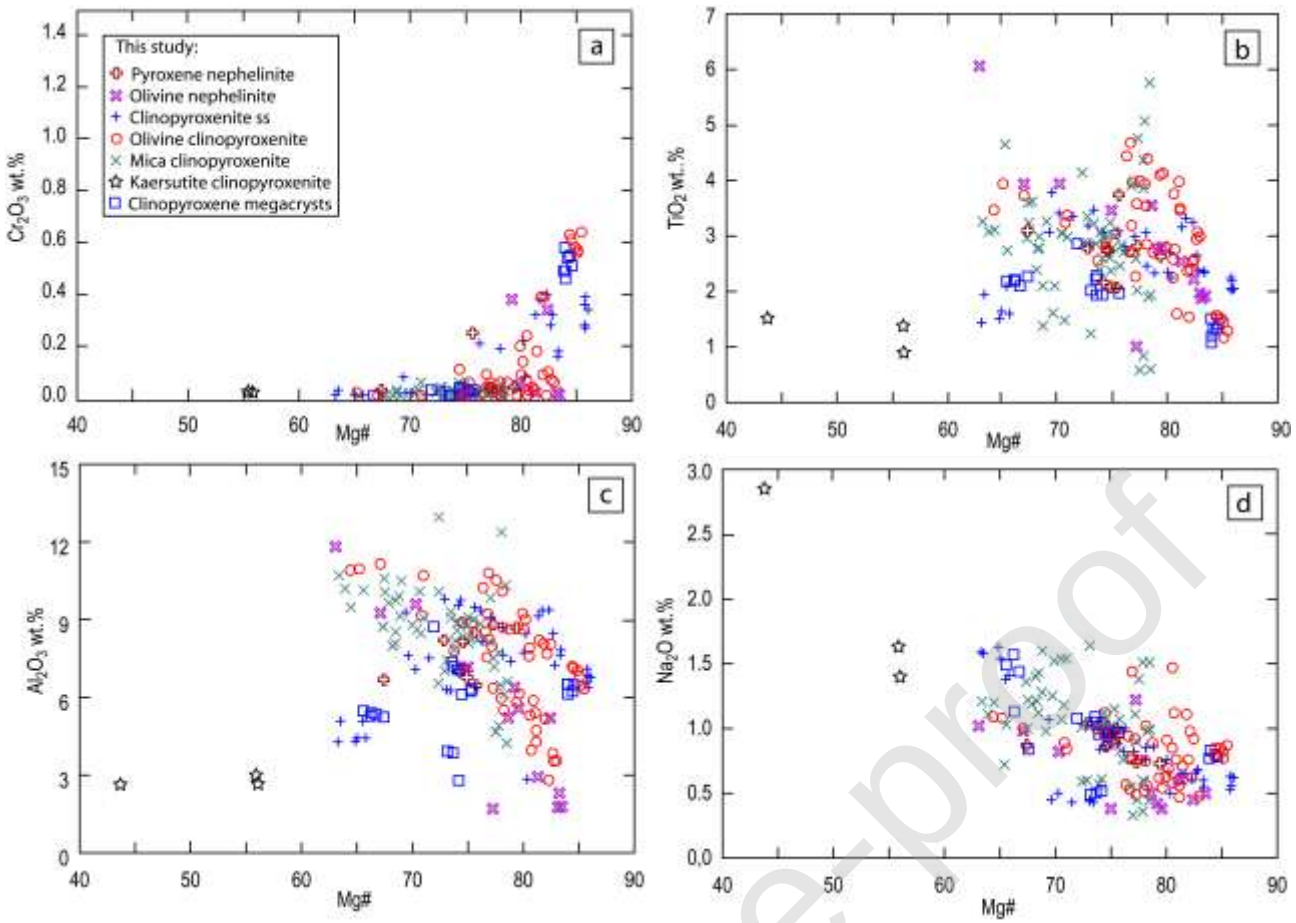

Fig. 5: a) Plot of Cr_2O_3 wt.% versus Mg# [100×Mg/(Mg+Fe_{tot})] in Cpx of pyroxenite xenoliths, megacrysts and nephelinites from JSVF; b) Plot of TiO_2 wt. % versus Mg# [100×Mg/(Mg+Fe_{tot})]; c) Plot of Al_2O_3 wt.% versus Mg# [100×Mg/(Mg+Fe_{tot})]; d) Plot of NaO wt.% versus Mg# [100×Mg/(Mg+Fe_{tot})].

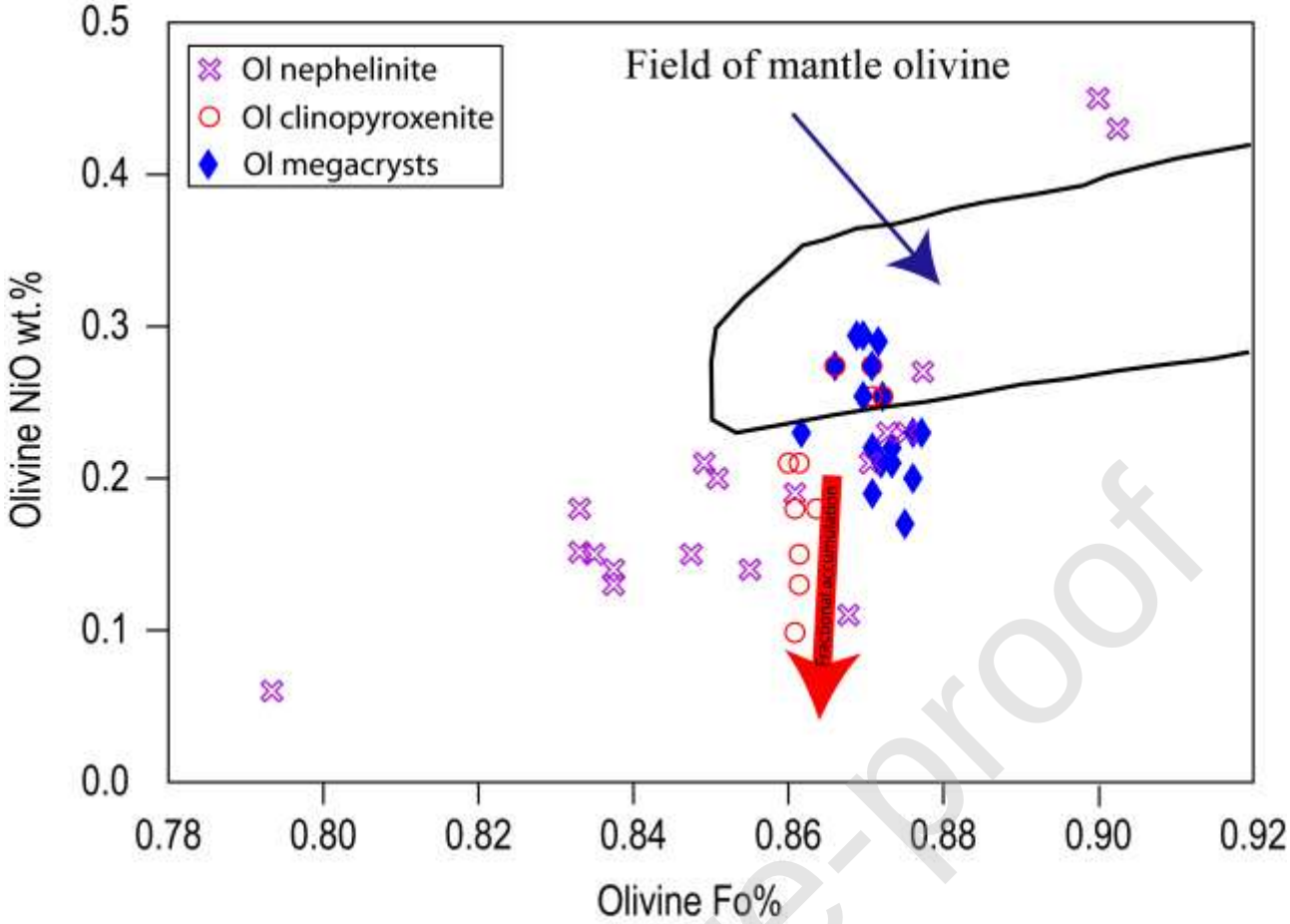

Fig. 6: Plot of Fo % versus NiO wt.% in olivine from olivine nephelinites, olivine pyroxenite xenoliths, and olivine megacrysts. Olivine mantle field from Takahashi (1987).

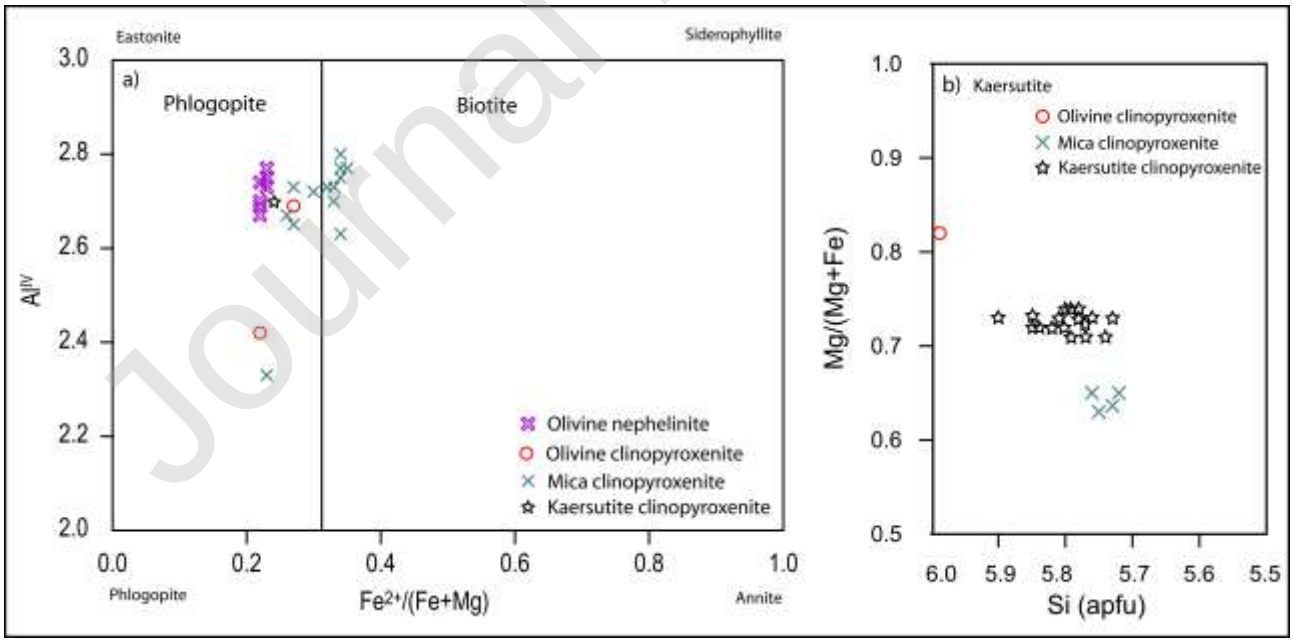

Fig. 7: a) Diagram of micas from the olivine nephelinites and pyroxenite xenoliths (Speer, 1984); b) Diagram of amphiboles from pyroxenite xenoliths (Leake et al., 1997).

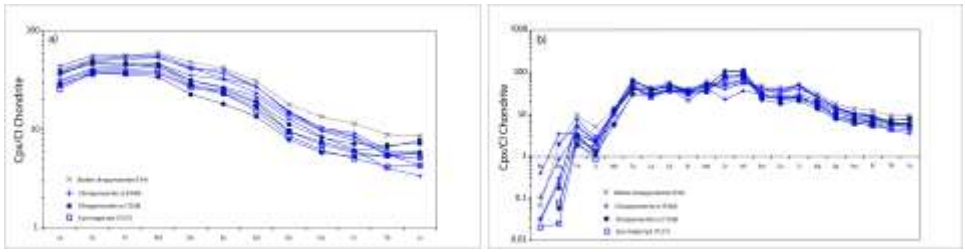

Fig 8: a) Chondrite-normalized REE patterns for clinopyroxenes in the pyroxenite xenoliths and megacrysts. Normalization values are from McDonough and Sun (1995); b) Chondrite-normalized incompatible trace element patterns for clinopyroxenes in the pyroxenite xenoliths and megacrysts. Normalization values are from McDonough and Sun (1995).

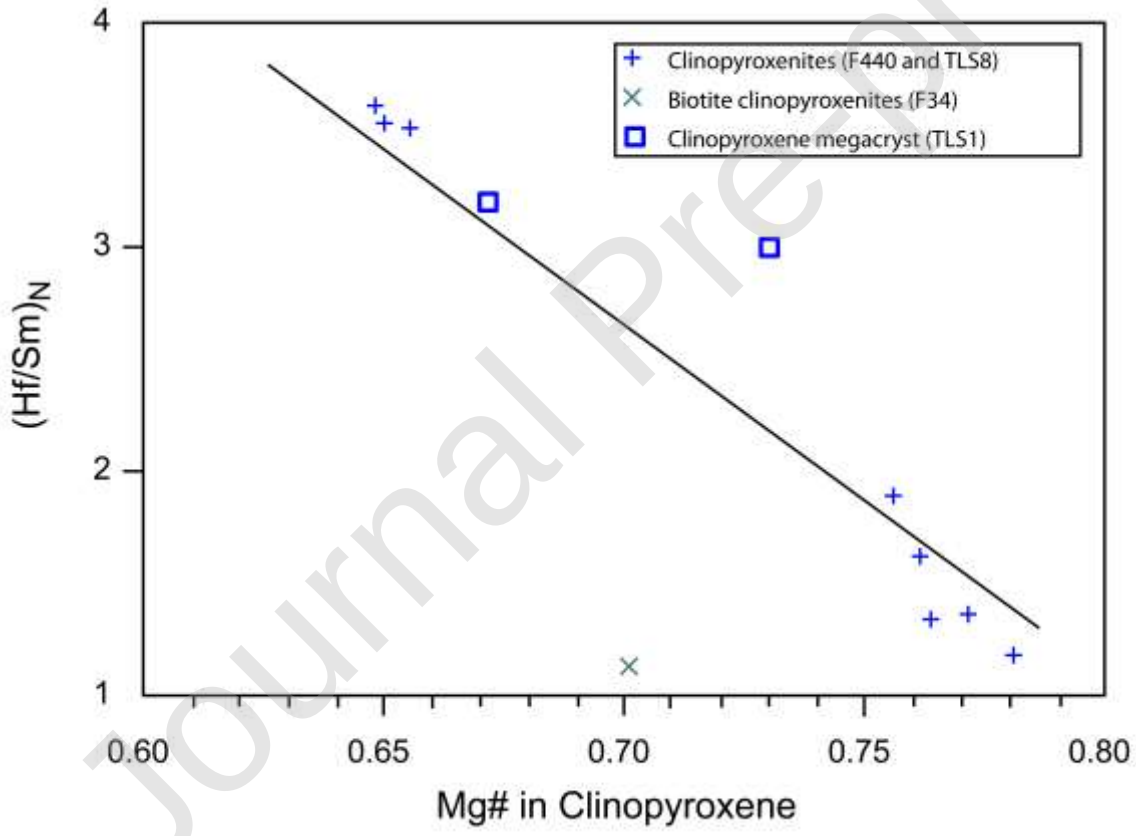

Fig. 9: Plot of Hf/Sm ratios versus Mg# for the clinopyroxenes in pyroxenite xenoliths and megacrysts.

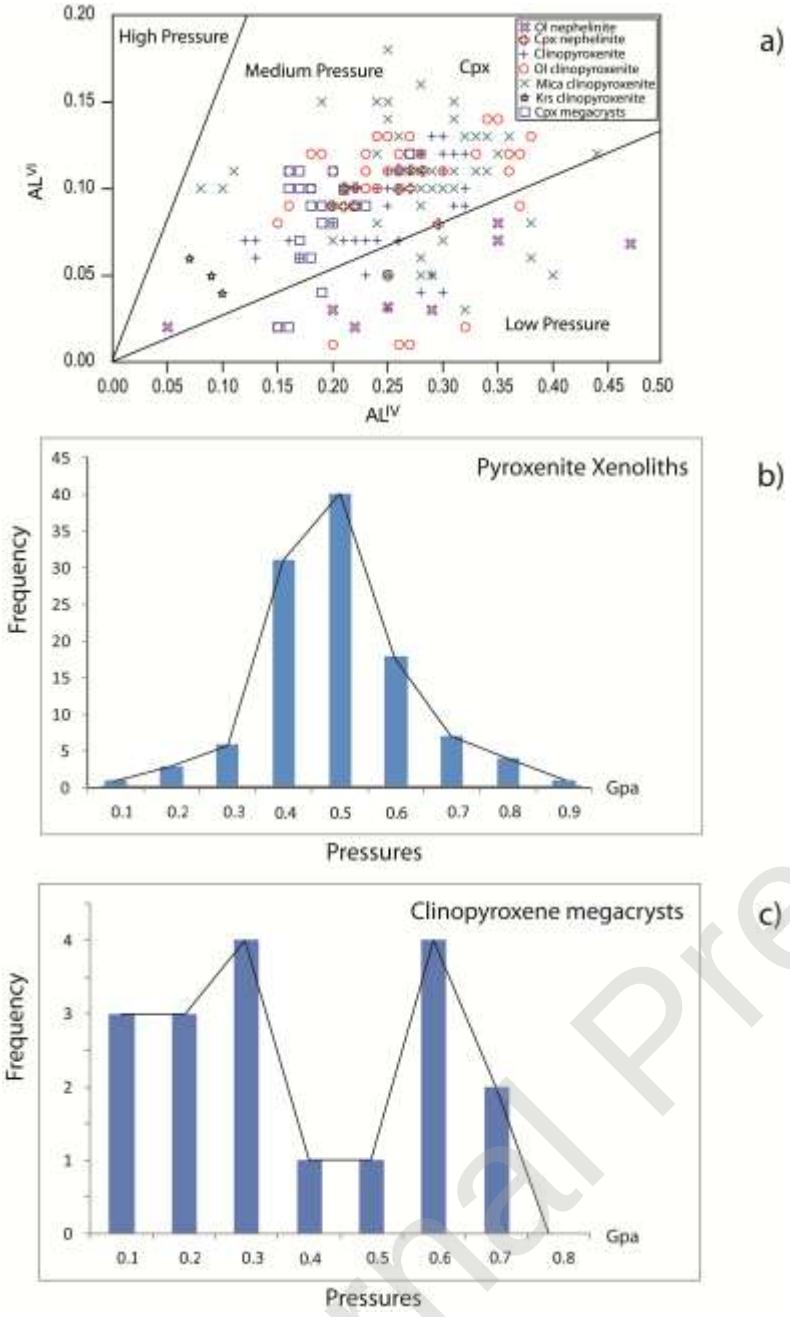

Fig. 10: a) Composition of the clinopyroxene of host rocks, pyroxenite xenoliths, and Cpx megacrysts in $Al^{(VI)}$versus$Al^{(IV)}$ diagram (after Aoki and Shiba, 1973); b and c). Histograms of pressure estimates of pyroxenite xenoliths and clinopyroxene megacrysts from JSVF. The pressure estimates in this study based mainly on clinopyroxene barometry (Nimis and Ulmer, 1998).

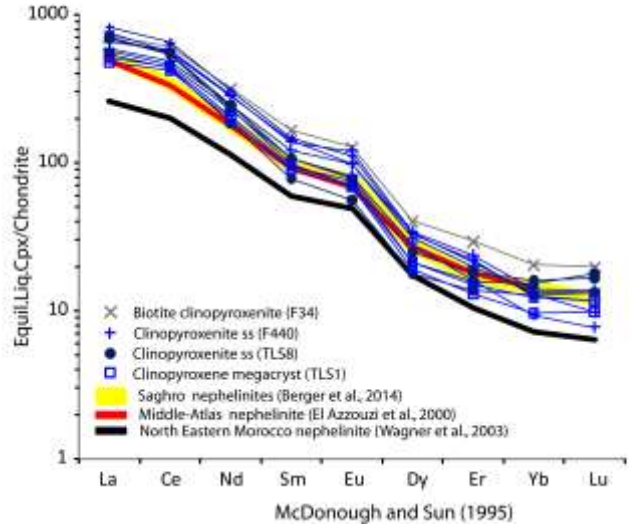

Fig. 11: Hypothetical melts in equilibrium with clinopyroxenes from pyroxenite xenoliths and Cpx megacrysts compared to host nephelinites (Berger et al. 2014). Normalizing values are from McDonough and Sun (1995). The Cpx/alkaline melt partition coefficients from Hart and Dunn (1993).

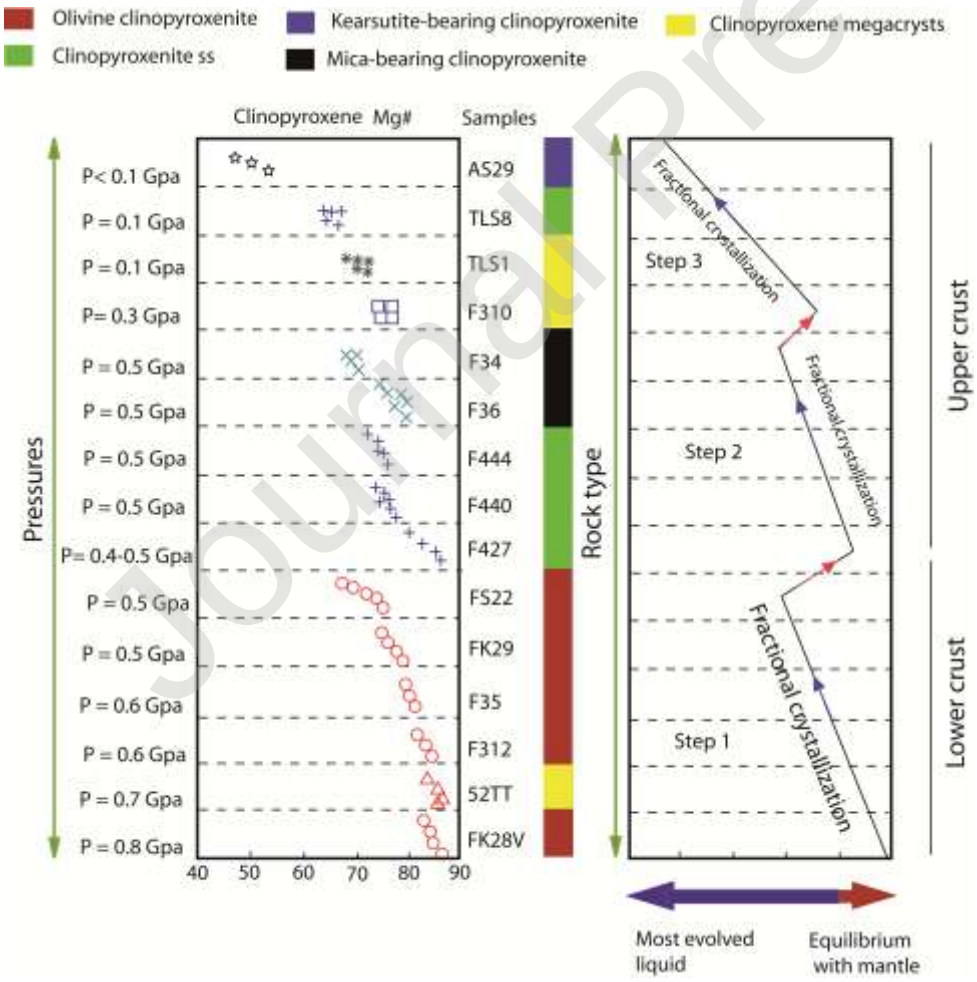

Fig. 12. A sketch showing variation of Mg-number in clinopyroxenes as a function of pressure as well the sequential crystallization for all pyroxenites and Cpx megacrysts from the same melts at crustal depths beneath the JSVF.

Table 1. Textures and modal compositions of pyroxenite xenoliths from Jbel Saghro

			Primary phases		Hydrous phases		Accessory phases							
Sample Number	Lithology	Texture	Ol	Cpx	Amp	Phl	Spl	Spn	Nph	Mag	Cb	Zeo	Other	Total
F34	Mica-bearing clinopyroxenite	Adcumulate	0	60	4	34	0	0	0	2	0	0	0	100
F36	Mica-bearing clinopyroxenite	Adcumulate	0	64	2	14	0	0	0	20	0	0	0	100
FS22	Olivine Clinopyroxenite	Orthocumulate	15	75	0	0	0	0	0	7	0	0	3	100
FK29	Olivine Clinopyroxenite	Adcumulate	16	70	0	2	0	0	1	2	0	2	7	100
F35	Olivine Clinopyroxenite	Orthocumulate	25	50	0	0	0	0	0	4	3	0	18	100
F312	Olivine Clinopyroxenite	Orthocumulate	20	60	2	0	0	0	1	7	0	0	10	100
FK28V	Olivine Clinopyroxenite	Poikilitic (Heteradcumulate)	40	48	0	0	1	0	1	3	5	0	2	100
TLS8	Clinopyroxenite ss	Adumulate	2	80	0	0	0	3	0	7	2	0	6	100
F440	Clinopyroxenite ss	Orthocumulate	0	75	0	0	0	0	0	0	0	5	20	100
F444	Clinopyroxenite ss	Adcumulate	0	93	0	4	0	0	0	3	0	0	0	100
F427B	Clinopyroxenite ss	Adcumulate	0	98	0	0	0	0	0	0	0	0	2	100
AS29	Kaersutite-bearing clinopyroxenite	Doleritic	0	32	30	20	0	0	0	4	4	0	10	100

Abbreviations: Ol, olivine; Cpx, clinopyroxene; Spl, spinel; Amp, amphibole; Phl, phlogopite; Spn, sphene (Titanite); Nph, nepheline; Mag, magnetite; Cb, carbonate; Zeo, zeolite.

Table 2. Representative major element compositions of clinopyroxenes from host nephelinites, pyroxenite xenoliths, and Cpx megacrysts from Jbel Saghro

Sample number	F310	TLS1	F444	F444	FK29	FK29	F34	F34	F34	F36	AS29	AS29	F310	F310	TLS1	TLS1	52TT	52TT
Rock Type	Nephelinite		Clinopyroxenite ss		Olivine clinopyroxenite		Mica-bearing clinopyroxenite				Kaersutite-bearing clinopyroxenite		Clinopyroxene megacrysts					
Mineral	Clinopyroxene																	
Crystal size	Phenocryst	Phenocryst	Phenocryst	Phenocryst	Phenocryst	Phenocryst	Phenocryst	Phenocryst	Phenocryst	Phenocryst	Phenocryst	Phenocryst	Phenocryst	Phenocryst	Phenocryst	Phenocryst	Phenocryst	Phenocryst
Location in crystal	Core	Rim	Rim	Core	Rim	Core	Core	Core	Rim	Rim			Core	Rim	Rim	Core	Core	Rim
Analysis No	30	58	57	58	20	21	25	22	56	122	100	102	36	37	70	75	91	92
Locality	Foum el kouss	Tlassem	Foum el kouss		Foum el kouss		Foum el kouss				Assaka		Foum el kouss		Tlassem		Tazlaft Tamzant	
Wt.%																		
SiO_2	47.92	45.01	45.86	46.85	47.24	46.82	46.04	42.49	40.86	45.37	49.08	49.11	47.99	48.50	48.53	48.92	49.60	49.54
TiO_2	2.06	3.46	3.47	2.86	2.58	2.37	2.60	5.76	4.37	2.83	1.24	1.38	1.98	2.02	2.21	2.02	1.51	1.42
Al_2O_3	6.69	7.17	6.27	6.29	7.91	8.08	6.85	10.20	12.38	8.48	2.91	2.86	6.31	6.30	5.28	3.92	6.52	6.47
Cr_2O_3	0.01	0.01	0.00	0.04	0.24	0.39	0.01	0.01	0.01	0.00	0.01	0.00	0.02	0.03	0.00	0.00	0.58	0.51
FeO	7.16	7.17	7.58	7.69	5.33	4.97	7.39	5.73	5.60	6.64	12.95	16.11	7.06	7.12	9.86	8.16	4.99	4.75
MnO	0.10	0.06	0.15	0.12	0.07	0.10	0.20	0.08	0.06	0.04	0.37	0.52	0.12	0.17	0.20	0.22	0.03	0.08
MgO	11.91	12.06	11.74	11.70	12.39	12.55	11.89	11.67	11.06	11.71	9.25	7.02	12.09	12.16	10.84	12.46	14.67	14.64
NiO	0.05	0.00					0.01	0.02	0.00	0.01	0.00	0.02	0.00	0.06	0.00	0.00	0.06	0.06
CaO	22.62	23.69	23.27	23.46	21.65	22.93	23.53	23.26	23.75	22.81	21.67	18.86	22.82	22.90	21.72	23.74	21.64	21.51
Na_2O	1.01	0.38	0.44	0.44	1.47	1.11	0.61	0.44	0.36	0.83	1.47	2.89	0.95	0.95	1.57	0.49	0.83	0.78
K_2O	0.01	0.01	0.02	0.01	0.11	0.05							0.01	0.00	0.00	0.02		
ZnO	0.07	0.00																
Total	99.60	99.02	98.91	99.46	98.99	99.36	99.12	99.66	98.44	98.72	98.96	98.78	99.34	100.21	100.25	100.02	100.43	99.76
Cations on the basis of 6 (O)																		
Si	1.799	1.713	1.749	1.771	1.768	1.749	1.748	1.600	1.559	1.720	1.903	1.929	1.805	1.808	1.830	1.842	1.817	1.824
Ti	0.058	0.099	0.100	0.081	0.072	0.067	0.074	0.163	0.125	0.081	0.036	0.041	0.056	0.057	0.063	0.057	0.042	0.039
Al	0.296	0.321	0.282	0.280	0.349	0.356	0.307	0.453	0.557	0.379	0.133	0.132	0.279	0.277	0.235	0.174	0.282	0.281
Cr	0.000	0.000	0.000	0.001	0.007	0.011	0.000	0.000	0.000	0.000	0.000	0.000	0.001	0.001	0.000	0.000	0.017	0.015
Fe	0.225	0.228	0.242	0.243	0.167	0.155	0.235	0.180	0.179	0.211	0.420	0.529	0.222	0.222	0.311	0.257	0.153	0.146
Mn	0.003	0.002	0.005	0.004	0.002	0.003	0.007	0.003	0.002	0.001	0.012	0.017	0.004	0.005	0.006	0.007	0.001	0.003
Mg	0.666	0.684	0.667	0.659	0.691	0.699	0.673	0.655	0.630	0.662	0.534	0.411	0.678	0.676	0.610	0.700	0.801	0.804
Ni	0.001	0.000	0.000	0.000	0.000	0.000	0.000	0.001	0.000	0.000	0.000	0.001	0.000	0.002	0.000	0.000	0.002	0.002
Ca	0.910	0.966	0.951	0.950	0.868	0.918	0.957	0.939	0.971	0.926	0.900	0.794	0.919	0.915	0.878	0.958	0.849	0.849
Na	0.074	0.028	0.033	0.032	0.107	0.080	0.045	0.032	0.026	0.061	0.111	0.220	0.069	0.068	0.115	0.036	0.059	0.056

K	0.000	0.000	0.001	0.001	0.005	0.002	0.000	0.000	0.000	0.000	0.000	0.000	0.000	0.000	0.000	0.001	0.000	0.000
Total	4.032	4.042	4.028	4.023	4.037	4.042	4.046	4.0	4.0	4.0	4.050	4.1	4.034	4.031	4.047	4.032	4.0	4.0
Al^{IV}	0.201	0.287	0.251	0.229	0.232	0.251	0.252	0.400	0.441	0.280	0.097	0.071	0.195	0.192	0.170	0.158	0.183	0.176
Al^{VI}	0.094	0.034	0.030	0.051	0.117	0.105	0.055	0.053	0.116	0.099	0.036	0.061	0.084	0.085	0.065	0.016	0.098	0.104
En	37.000	36.432	35.884	35.586	40.043	39.446	36.097	36.936	35.380	36.794	28.818	23.713	37.264	37.287	33.897	36.548	44.430	44.691
Wo	50.521	51.420	51.120	51.292	50.286	51.788	51.326	52.897	54.576	51.504	48.538	45.767	50.529	50.463	48.817	50.029	47.091	47.182
Fs	12.479	12.148	12.996	13.123	9.671	8.766	12.577	10.166	10.044	11.703	22.644	30.520	12.208	12.249	17.285	13.422	8.479	8.127
Mg#	74.78	74.99	73.41	73.06	80.55	81.82	74.16	78.42	77.89	75.87	56.00	43.72	75.32	75.27	66.23	73.14	83.97	84.61

Mg# = molar
mg/(mg+Fe)*100.

Table 3. Representative major element compositions of olivines from olivine nephelinites, olivine clinopyroxenites, and olivine megacrysts from Jbel Saghro

Sample number	TLS1	TLS1	F423	F423	F1I	FK28	FS22	FS22	FK29	FK29	FK28V	F423	F423	F1I	F1I
Host rock or xenolith	Olivine nephelinite					Olivine clinpyroxenite						Olivine megacrysts			
Mineral	Olivine														
Crystal size	Phenocryst	Phenocryst	Phenocryst	Phenocryst	Phenocryst	Phenocryst	Phenocryst	Phenocryst	Phenocryst	Phenocryst	Phenocryst	Megacryst	Megacryst	Megacryst	Megacryst
Location in crystal	Rim	Rim	Rim	Core	Core	Rim	Rim	Core	Rim	Core	Core	Rim	Core	Rim	Core
Analysis No	56	68	129	130	97	4	11	12	28	29	52	138	143	98	101
Locality	Tlassem		Foum el kouss			Foum el kouss						Foum el kouss			
Wt.%															
SiO_2	40.62	41.19	38.96	40.57	40.21	40.57	40.82	40.04	40.43	40.18	40.52	40.70	40.96	39.96	39.98
TiO_2	0.03	0.00	0.05	0.02	0.03	0.00	0.01	0.01	0.03	0.03	0.00	0.03	0.02	0.03	0.01
Al_2O_3	0.04	0.00	0.38	0.03	0.10	0.04	0.07	0.04	0.06	0.08	0.04	0.07	0.05	0.07	1.88
Cr_2O_3	0.01	0.03	0.02	0.06	0.03	0.03	0.04	0.05	0.00	0.02	0.02	0.05	0.03	0.02	0.03
FeO	15.68	9.70	18.16	12.33	11.94	13.20	12.40	11.95	14.61	14.05	13.00	11.80	12.24	12.61	12.51
MnO	0.23	0.19	0.92	0.21	0.14	0.23	0.03	0.29	0.13	0.12	0.15	0.16	0.17	0.16	0.17
MgO	44.33	49.22	39.38	46.70	47.08	45.91	45.03	45.59	44.58	44.85	46.19	47.21	46.61	45.67	45.24
NiO	0.15	0.45	0.06	0.21	0.23	0.10	0.27	0.25			0.18	0.23	0.21	0.27	0.27
CaO	0.16	0.05	0.96	0.30	0.47	0.25	0.23	0.20	0.44	0.45	0.26	0.22	0.26	0.19	0.19
Na_2O	0.02	0.04	0.01	0.04	0.02	0.01	0.04	0.01	0.02	0.00	0.01	0.04	0.03	0.00	0.06
K_2O	0.03	0.00	0.00	0.00	0.01				0.00	0.00		0.03	0.01	0.02	0.04
ZnO	0.02	0.00	0.12	0.00	0.00										
Total	101.30	100.86	99.01	100.46	100.24	100.35	98.94	98.43	100.29	99.77	100.37	100.53	100.60	99.06	100.42
Cations on the basis of 4 (O)															
Si	1.009	1.001	1.009	1.002	0.995	1.005	1.020	1.007	1.008	1.005	1.003	1.002	1.009	1.003	0.988
Ti	0.001	0.000	0.001	0.000	0.000	0.000	0.000	0.000	0.001	0.000	0.000	0.001	0.000	0.001	0.000
Al	0.001	0.000	0.012	0.001	0.003	0.001	0.002	0.001	0.002	0.002	0.001	0.002	0.001	0.002	0.055
Cr	0.000	0.001	0.000	0.001	0.001	0.001	0.001	0.001	0.000	0.000	0.000	0.001	0.001	0.000	0.000
Fe	0.326	0.197	0.393	0.255	0.247	0.274	0.259	0.251	0.305	0.294	0.269	0.243	0.252	0.265	0.258
Mn	0.005	0.004	0.020	0.004	0.003	0.005	0.001	0.006	0.003	0.003	0.003	0.003	0.004	0.003	0.003
Mg	1.641	1.784	1.521	1.720	1.737	1.696	1.678	1.710	1.658	1.672	1.705	1.733	1.711	1.710	1.667
Ni	0.003	0.009	0.001	0.004	0.005	0.002	0.005	0.005	0.000	0.000	0.003	0.005	0.004	0.005	0.005
Ca	0.004	0.001	0.027	0.008	0.012	0.007	0.006	0.005	0.012	0.012	0.007	0.006	0.007	0.005	0.005
Na	0.001	0.002	0.001	0.002	0.001	0.000	0.002	0.001	0.001	0.000	0.001	0.002	0.001	0.000	0.003
K	0.001	0.000	0.000	0.000	0.000	0.000	0.000	0.000	0.000	0.000	0.000	0.001	0.000	0.001	0.001
Total	2.991	2.999	2.984	2.997	3.003	2.991	2.974	2.988	2.988	2.989	2.993	2.997	2.991	2.995	2.986
Fo %	83.44	90.05	79.45	87.10	87.55	86.11	86.62	87.18	84.48	85.05	86.37	87.71	87.16	86.59	86.58

Fo % = molar mg/(mg+Fe)*100.

Table 4. Representative major element compositions of amphiboles and micas from pyroxenite xenoliths and host nephelinites from Jbel Saghro

Sample Number	F34	F34	F34	F34	AS29	AS29	AS29	F312	F34	F34	F36	F36	FK29	FK29	AS29	F1I	F1I
Host rock or xenolith	Mica-bearing clinopyroxenite				Kaersutite-bearing clinopyroxenite			Olivine clinopyroxenite	Mica-bearing clinopyroxenite				Olivine clinopyroxenite		Kaersutite-bearing clinopyroxenite	Olivine nephelinite	
Mineral	Amphibole				Amphibole				Mica				Phlogopite			Phlogopite	
Crystal size	Phenocryst	Phenocryst	Phenocryst	Phenocryst	Phenocryst	Phenocryst	Phenocryst	Phenocryst	Phenocryst	Phenocryst	Phenocryst	Phenocryst	Phenocryst	Phenocryst	Phenocryst	Phenocryst	Phenocryst
Location in crystal	Rim	Core	Rim	Core	Rim	Core	Rim		Rim	Core	Rim	Rim	Rim	Rim	Core	Core	Rim
Analysis No	6	7	8	9	70	71	76	54	10	11	135	137	19	22	85	116	117
Locality	Foum el kouss				Assaka			Foum el kouss	Foum el kouss				Foum el kouss		Assaka	Foum el kouss	
Wt.%																	
SiO_2	38.21	37.88	38.11	38.06	38.80	38.72	39.04	40.47	35.22	35.89	37.30	34.83	35.40	38.37	36.30	36.10	35.96
TiO_2	5.26	4.78	4.99	4.16	5.83	5.63	5.77	5.93	5.44	5.56	4.99	5.47	6.13	3.51	6.82	6.31	6.53
Al_2O_3	14.87	14.75	14.69	15.06	13.23	13.35	12.94	12.25	16.56	15.97	18.93	17.23	15.71	16.70	15.85	15.94	16.06
Cr_2O_3	0.00	0.02	0.03	0.02	0.12	0.10	0.00	0.19	0.03	0.03	0.07	0.00	0.02	0.00	0.08	0.02	0.00
FeO	11.16	11.40	10.81	11.76	8.91	8.89	8.95	6.02	11.48	10.29	9.54	9.72	10.38	8.68	9.26	8.89	9.15
MnO	0.14	0.06	0.07	0.05	0.00	0.08	0.07	0.06	0.16	0.01	0.00	0.00	0.00	0.14	0.08	0.08	0.05
MgO	11.49	11.47	11.51	11.39	13.92	13.76	14.07	14.98	15.09	16.59	14.44	14.41	16.15	16.84	16.89	17.42	17.56
NiO																0.04	0.04
CaO	11.98	11.76	11.84	11.78	12.15	12.25	12.37	12.29	0.01	0.03	0.05	0.09	0.00	0.25	0.05	0.02	0.01
Na_2O	1.97	2.07	1.94	2.15	2.10	2.07	2.16	2.08	0.41	0.14	1.87	0.42	0.04	2.55	1.05	1.05	1.07
K_2O	2.54	2.67	2.65	2.59	1.95	2.01	1.93	1.75	9.47	9.67	10.08	11.01	9.50	7.46	8.64	8.43	8.59
Total	97.69	96.89	96.89	97.09	97.44	96.87	97.30	97.08	94.11	95.12	101.04	97.05	96.34	95.74	95.94	94.37	95.02
Cations on the basis of 23 (O) for amphibole																	
Cations on the basis of 22 (O) for mica																	
Si	5.722	5.730	5.757	5.749	5.779	5.780	5.803	5.987	5.284	5.331	5.347	5.267	5.310	5.571	5.304	5.301	5.254
Ti	0.592	0.544	0.567	0.473	0.654	0.632	0.645	0.660	0.614	0.621	0.538	0.622	0.691	0.383	0.749	0.697	0.717
Al	2.625	2.629	2.616	2.682	2.323	2.349	2.267	2.136	2.929	2.797	3.198	3.070	2.777	2.857	2.730	2.758	2.766
Cr	0.000	0.002	0.003	0.002	0.014	0.012	0.000	0.022	0.004	0.003	0.008	0.000	0.002	0.000	0.010	0.002	0.000
Fe	1.398	1.442	1.366	1.486	1.110	1.110	1.112	0.744	1.440	1.278	1.144	1.229	1.302	1.053	1.132	1.092	1.118
Mn	0.017	0.008	0.009	0.006	0.000	0.010	0.009	0.007	0.020	0.001	0.000	0.000	0.000	0.017	0.010	0.009	0.006
Mg	2.566	2.588	2.593	2.565	3.091	3.063	3.119	3.305	3.376	3.676	3.087	3.249	3.612	3.645	3.681	3.814	3.825
Ni	0.000	0.000	0.000	0.000	0.000	0.000	0.000	0.000	0.000	0.000	0.000	0.000	0.000	0.000	0.000	0.004	0.005
Ca	1.922	1.907	1.917	1.907	1.939	1.959	1.970	1.947	0.001	0.005	0.008	0.014	0.000	0.040	0.008	0.003	0.002
Na	0.571	0.608	0.569	0.630	0.607	0.599	0.623	0.596	0.120	0.041	0.521	0.124	0.010	0.719	0.296	0.299	0.303
K	0.485	0.515	0.511	0.498	0.371	0.383	0.366	0.331	1.813	1.833	1.844	2.125	1.819	1.382	1.611	1.580	1.602

Total	15.901	15.972	15.907	16.000	15.888	15.898	15.914	15.737	15.602	15.585	15.695	15.701	15.524	15.667	15.530	15.561	15.598
Mg#	64.73	64.21	65.50	63.32	73.57	73.40	73.71	81.62	70.10	74.20	72.97	72.55	73.50	77.58	76.48	77.74	77.38

Mg# = molar mg/(mg+Fe)*100.

Table 5. Representative major element compositions of accessory phases (Titanite, Ti-magnetite, spinel, rhönite, nepheline, feldspar, and carbonate) of pyroxenite xenoliths from Jbel Saghro

Sample Number	TLS8	TLS8	TLS8	TLS8	FK28V	FK28V	FK28V	FK28V	FK28V	TLS8	TLS8	AS29	AS29	FS22	F310	F310	F312	F312
Host rock or xenolith	Clinopyroxinite ss				Olivine clinopyroxenite					Clinopyroxenite ss		Kaersutite-bearing clinopyroxenite		Olivine clinopyroxenite	Cpx megacrysts		Olivine clinopyroxenite	
Mineral	Titanite				Spinel					Ti-magnetite							Rhonite	
Crystal size	Phenocryst	Phenocryst	Phenocryst	Phenocryst	Phenocryst	Phenocryst	Phenocryst	Phenocryst	Phenocryst	Phenocryst	Phenocryst	Phenocryst	Phenocryst	Phenocryst	Inclusion	Iinclusion	Phenocryst	Phenocryst
Analysis No	10	11	12	13	9	10	55	56	57	4	5	107	108	15	46	47	55	56
Locality	Tlassem				Foum el kouss					Tlassem		Assaka		Foum el kouss	Foum el kouss		Foum el kouss	
wt.%																		
SiO_2	29.94	29.83	29.77	29.78	0.10	0.05	0.48	0.08	0.04	0.06	0.08	0.07	0.05	0	0.01	0.00	26.20	25.66
TiO_2	37.17	37.32	37.83	37.87	1.45	1.56	1.86	1.61	1.36	10.83	10.97	14.73	14.86	13.85	15.77	16.39	8.18	8.00
Al_2O_3	1.25	1.32	0.88	1.06	34.29	34.51	32.76	32.14	39.49	2.81	2.79	1.99	2.19	0.37	0.33	0.45	15.73	16.17
Cr_2O_3	0.00	0.03	0.01	0.01	24.18	23.64	25.13	27.18	19.57	0.00	0.01	1.72	2.16	0.64	0.03	0.05	0.15	0.15
FeO	1.13	1.28	0.83	0.76	23.70	23.88	22.79	21.71	21.03	77.37	76.94	70.20	70.47	73.04	72.05	72.20	16.07	16.90
MnO	0.02	0.07	0.05	0.06	0.20	0.12	0.20	0.12	0.27	0.93	0.97	0.99	0.88	1.64	1.32	1.33	0.11	0.07
MgO	0.02	0.03	0.00	0.00	15.08	15.12	15.10	15.34	16.99	2.77	2.70	4.47	4.42	4.93	4.94	4.91	16.93	16.62
NiO					0.16	0.08	0.13	0.11	0.12			0.08	0.04	0.09	0.07	0.06		
CaO	27.81	27.82	27.43	27.90	0.01	0.03	0.05	0.01	0.04	0.04	0.01	0.04	0.09	0.08	0.55	0.23	11.75	11.53
Na_2O	0.05	0.07	0.08	0.05	0.01	0.00	0.01	0.01	0.00	0.02	0.01	0	0	0	0.043	0.033	1.31	1.30
K_2O	0.03	0.01	0.01	0.00						0.00	0.01				0.019	0.016	0.03	0.00
Total	97.42	97.77	96.89	97.50	99.18	98.99	98.51	98.31	98.91	94.84	94.48	94.28	95.15	94.63	95.31	95.71	96.48	96.50
Spinel and Ti-magnetite: Cation on the basis on 4 (O)																		
Si	1.097	1.000	1.097	1.097	0.003	0.001	0.014	0.002	0.001	0.003	0.003	0.003	0.002	0.000	0.000	0.000	3.329	3.889
Ti	0.838	0.941	0.838	0.838	0.032	0.034	0.041	0.036	0.029	0.410	0.306	0.410	0.410	0.385	0.436	0.451	0.782	0.912
Al	0.074	0.052	0.074	0.074	1.173	1.181	1.132	1.115	1.313	0.087	0.122	0.087	0.094	0.016	0.014	0.019	2.356	2.888
Cr	0.000	0.001	0.000	0.000	0.555	0.543	0.583	0.633	0.436	0.050	0.000	0.050	0.063	0.019			1.614	0.018
Fe	0.028	0.036	0.028	0.028	0.270	0.269	0.221	0.245	0.215									
Mn	0.001	0.002	0.001	0.001	0.005	0.003	0.005	0.003	0.006	0.031	0.031	0.031	0.027	0.051	0.041	0.041	1.265	0.009
Mg	0.000	0.001	0.000	0.000	0.652	0.655	0.660	0.673	0.714	0.247	0.149	0.247	0.241	0.271	0.270	0.268	0.248	3.755
Ni	0.000			0.000	0.004	0.002	0.003	0.003	0.003								0.000	0.000
Ca	0.989	0.999	0.989	0.989	0.000	0.001	0.002	0.000	0.001	0.001	0.001	0.001	0.003	0.003	0.022	0.009	1.600	1.872
Na	0.000	0.004	0.000	0.000	0.000	0.000	0.001	0.001	0.000	0.000	0.000	0.000	0.000	0.000	0.003	0.002	0.322	0.383
Fe2+	0.028	0.036	0.028	0.028						1.133	1.128	1.133	1.140	1.059	1.097	1.128	0.035	0.000

Fe3+					0.306	0.311	0.338	0.289	0.281	1.038	1.260	1.038	1.020	1.196	1.116	1.080	1.672	2.141
Total	3.000	3.036	3.028	3.000	3.000	3.000	3.000	3.000	3.000	3.000	3.000	3.000	3.000	3.000	3.000	3.000	20.000	20.000
Mg#					70.74	70.91	74.96	73.28	76.85									
Cr#					32.12	31.48	33.97	36.20	24.95									
% ülvospinel										44.110	32.706	44.110	44.546	39.12961947	43.842	45.500		

Table 5 (continued)

Sample Number	F312	F1I	F1I	TLS1	F35	F35
Host rock or xenolith	Olivine clinopyroxenite	Olivine megacryst	Olivine megacryst	Clinopyroxene megacryst	Olivine clinopyroxenite	
Mineral	Nepheline		Feldspar	Carbonate		
Crystal size	Phenocryst	Inclusion	Inclusion	inclusion	Phenocryst	
Analysis No	50	118	107	61	109	110
Locality	Foum el kouss			Tlassem	Foum el kouss	
wt.%						
SiO_2	41.45	50.90	64.98	0.63	0.02	0.03
TiO_2	0.07	0.09	0.29	0.02	0.01	0.00
Al_2O_3	31.97	30.04	18.41	0.01	0.01	0.01
Cr_2O_3	0.00	0.01	0.00	0.00	0.00	0.00
FeO	2.30	1.11	0.69	0.06	0.00	0.02
MnO	0.00	0.01	0.00	0.02	0.00	0.00
MgO	0.03	0.23	0.00	0.09	1.34	1.50
NiO		0.02	0.00	0.00	0.00	0.01
CaO	0.30	0.31	0.09	53.72	54.70	55.80
Na_2O	15.26	16.18	3.29	0.38	0.05	0.02
K_2O	7.89	3.47	12.27	0.01	0.03	0.00
Total	99.262	102.40	100.06	54.99	56.16	57.40
Cation on the basis of 8 (O) for feldspar						
Si			3.06			
Ti			0.01			
Al			1.02			
Fe3+			0.00			
Fe2+						
Mn			0.00			
Mg			0.00			
Ca			0.00			
Na			0.30			
K			0.37			
Total			4.76			
Albite			44.59			
Anorthite			0.69			
Orthose			54.72			
Total			100.00			

Table 6. Representative clinopyroxene trace element analyses (LA-ICP-MS) of biotite-bearing clinopyroxenite, clinopyroxenite xenoliths, and Cpx megacrysts from Jbel Saghro (values in ppm)

Sample number	F34	F440	F440	F440	F440	TLS8	TLS8	TLS8	TLS1	TLS1
Xenolith type	Biotite-bearing clinopyroxenite	Clinopyroxenite ss				Clinopyroxenite ss			Clinopyroxene megacryst	
Locality	Foum el kouss					Tlassem				
Mineral	Clinopyroxene									
ppm										
Ti	22382.05	20820.52	17668.50	21240.36	13680.50	10844.74	9163.88	9905.66	11433.58	11903.58
Rb	0.157	0.07	<0,030	0.24	0.08	<0,029	<0,025	<0,027	0.047	<0,053
Sr	286.3	216.26	221.61	241.58	155.04	257.74	233.76	272.97	220.91	238.1
Zr	190.32	154.10	156.76	211.94	87.11	408.55	315.58	405.04	267.65	292.36
Nb	3.13	2.70	2.94	2.59	1.49	3.23	1.33	2.90	2.44	2.68
Ba	4.67	0.55	4.72	2.07	0.72	0.14	<0,062	0.42	0.061	0.184
La	9.09	10.42	9.69	7.56	7.25	8.97	6.83	8.78	6.13	6.58
Ce	32.25	34.10	29.95	25.59	24.14	28.96	22.70	28.23	22.53	23.56
Pr	5.19	5.12	4.80	4.06	3.77	4.38	3.35	4.16	3.46	3.55
Nd	27.48	26.26	24.29	21.20	19.61	20.99	15.67	20.01	16.78	17.93
Sm	7.15	6.33	6.21	5.21	4.61	4.64	3.37	4.23	3.94	4.1
Eu	2.38	2.07	1.84	1.82	1.51	1.46	1.02	1.32	1.3	1.4
Gd	6.12	5.38	5.40	4.66	4.26	3.83	2.69	3.37	3.08	3.68
Tb	0.815	0.72	0.66	0.62	0.54	0.51	0.34	0.42	0.392	0.447
Dy	4.41	3.57	3.66	3.39	3.11	2.75	1.94	2.33	2.1	2.34
Ho	0.731	0.57	0.54	0.53	0.46	0.45	0.32	0.41	0.338	0.383
Er	1.83	1.36	1.33	1.23	0.99	1.13	0.85	0.98	0.81	0.93
Tm	0.241	0.16	0.15	0.14	0.12	0.15	0.11	0.14	0.093	0.135
Yb	1.416	0.87	0.90	0.93	0.65	1.12	0.88	1.06	0.674	0.86
Lu	0.212	0.125	0.105	0.141	0.0824	0.177	0.14	0.19	0.106	0.126
Hf	5.63	5.93	5.78	6.86	3.77	11.38	8.51	10.4	8.22	9.12
Ta	0.709	0.803	0.906	0.54	0.403	0.888	0.405	0.534	0.595	0.65
Pb	0.167	0.0364	0.0497	0.0561	0.029	0.12	0.0991	0.093	0.0827	0.098
Th	0.274	0.216	0.157	0.1022	0.144	0.0876	0.0527	0.095	0.066	0.067
U	0.037	0.0213	0.0175	0.0165	0.0167	0.0087	0.0085	0.0094	0.0065	0.0121
Trace elements ratios:										
La (N)	38.35	43.97	40.89	31.90	30.59	37.85	28.82	37.05	25.86	27.76
Yb (N)	8.80	5.40	5.61	5.75	4.06	6.95	5.47	6.59	4.19	5.34
$(La/Yb)_N$	4.36	8.14	7.29	5.55	7.53	5.45	5.27	5.62	6.18	5.20
$(Ce/Yb)_N$	5.98	10.29	8.71	7.27	9.69	6.80	6.77	6.99	8.78	7.20

Table 7. Estimates of the equilibration pressures (GPa) of the investigated samples using Nimis and Ulmer (1998).

Rock type	Pyroxenite xenoliths	Clinopyroxene megacrysts			Nephelinites
Locality	Foum el kouss, Assaka and Tlassem	Tlassem	Foum el kouss	Tazlaft Tamzant	Foum el kouss and Tlassem
Equilibrium Pressures					
P (Gpa) (Nimis and Ulmer, 1998)	0.4-0.8	0.1	0.3	0.7	0.3-0.4